Alterations of redox dynamics and desmin post-translational modifications in skeletal muscle models of desminopathies

Florence Delort, Bertrand-David Segard, Coralie Hakibilen, Fany Bourgois-Rocha, Eva Cabet, Patrick Vicart, Meng-Er Huang, Guilhem Clary, Alain Lilienbaum, Onnik Agbulut, et al.

Research Article

Alterations of redox dynamics and desmin post-translational modifications in skeletal muscle models of desminopathies

Florence Delort[a], Bertrand-David Segard[a], Coralie Hakibilen[a], Fany Bourgois-Rocha[a], Eva Cabet[a], Patrick Vicart[a], Meng-Er Huang[b], Guilhem Clary [c], Alain Lilienbaum[a], Onnik Agbulut[d] , and Sabrina Batonnet-Pichon[a]

[a]Université de Paris, Unité de Biologie Fonctionnelle et Adaptative, CNRS UMR 8251, F-75013 Paris, FRANCE.

[b]Institut Curie, PSL Research University, CNRS UMR3348, Université Paris-Sud, Université Paris-Saclay, Orsay, 91405, France.

[c]Inserm U1016, Institut Cochin, CNRS UMR8104, Université Paris-Descartes, Sorbonne Paris Cité, Plateforme Protéomique 3P5, Paris, France.

[d]Sorbonne Université, Institut de Biologie Paris-Seine (IBPS), CNRS UMR 8256, Inserm ERL U1164, Biological Adaptation and Ageing, 75005, Paris, France.

Abbreviations: IF, intermediate filament; ROS, reactive oxygen species; WT, wildtype; PTM, post-translational modifications; NAC, N-acetyl-L-cysteine; GSSG, oxidized glutathione; GSH, reduced glutathione; AAV, adeno-associated-virus; TA, tibialis anterior; DMEM, Dulbecco's Modified Eagle's medium; HE, hematoxylin/eosin; SDH, succinate dehydrogenase

Abstract:

Desminopathies are a type of myofibrillar myopathy resulting from mutations in *DES*, encoding the intermediate filament protein desmin. They display heterogeneous phenotypes, suggesting environment influences. Patient muscle proteins show oxidative features linking oxidative stress, protein aggregation, and abnormal protein deposition. To improve understanding of redox balance in desminopathies, we further developed cellular models of four pathological mutants localized in 2B helical domain (the most important region for desmin polymerization) to explore desmin behavior upon oxidative stress. We show that the mutations desQ389P and desD399Y share common stress-induced aggregates, desR406W presents more scattered cytoplasmic aggregative pattern, and pretreatment with N-acetyl-L-cysteine (NAC), an antioxidant molecule, prevents all type of aggregation. Mutants desD399Y and desR406W had delayed oxidation kinetics following H_2O_2 stress prevented by N-acetyl-L-cysteine pretreatment. Further, we used AAV-injected mouse models to confirm *in vivo* effects of N-acetyl-L-cysteine. AAV-desD399Y-injected muscles displayed similar physio-pathological characteristics as observed in patients. However, after 2 months of N-acetyl-L-cysteine treatment, they did not have reduced aggregates. Finally, in both models, stress induced some post-translational modifications changing Isoelectric Point, such as potential hyperphosphorylations, and/or molecular weight of human desmin by proteolysis. However, each mutant presented its own pattern that seemed to be post-aggregative. In conclusion, our results indicate that individual desmin mutations have unique pathological molecular mechanisms partly linked to alteration of redox homeostasis. Integrating these mutant-specific behaviors will be important when considering future therapeutics.

Highlights

►Desmin mutations trigger variable aggregative patterns and NAC pretreatment avoids it.

►Desmin mutations induce delayed oxidation kinetic with H2O2 stress, which are prevented by NAC.

►Stresses induce own post-aggregative post-translational modifications, which are prevented by NAC.

►Distinct pathological molecular mechanisms of desmin mutations weigh on therapeutics.

Keywords: desmin, oxidative stress, aggregation, N-acetyl-L-cysteine, myopathies, intermediate filaments.

Introduction:

Desmin is a muscle-specific type III intermediate filament (IF). All IFs share a common tripartite organization characterized by a central alpha-helical coiled coil-forming region (rod-domain) and two non-alpha-helical regions (“head” and “tail”) with variable lengths and sequences (1) as represented for desmin in figure 1A. This structure allows protein monomers to assemble (2,3) and ultimately form networks within cells. Thus, desmin participates in cytoskeleton formation, crosslinking myofibrils and connecting them to mitochondria (4), nuclei, membrane desmosomal proteins in cardiac cells (2,3), or costamers in skeletal muscle (4,5).

Currently, ~70 mutations within the human desmin gene, *DES* (HUGO Gene Nomenclature Committee database #2770), lead to desminopathies, a subcategory

of myofibrillar myopathies that mostly arise between the second and fifth decade of life (6,7). Individuals with desminopathies present skeletal or cardiac muscle defects (8) that exhibit heterogeneous features, such as progressive skeletal myopathy (9), different types of cardiomyopathy (10), or both (11–14). The same point mutation can produce different phenotypes within a family, suggesting that genetic factors as well as environmental (such as intensive sport practice, alimentation, anxiety…) influence disease progression (15).

Most desmin mutations are missense and affect the 2B end of the protein rod central dimerization domain, leading to desmin network disorganization (16). The main histological characteristics are myofibrillar disorganization, sarcomere misalignment, and desmin-containing protein aggregates in the sarcoplasm. Many studies have investigated how desmin mutations affect the capacity of recombinant proteins to self-assemble in filaments *in vitro,* as well as in transient cell experiments with or without another IF (e.g., vimentin) (17). Indeed, several mutant monomers polymerize normally *in vitro*, while some present irregular-diameter filaments, such as desD399Y (17,18). For other mutants, the assembly process stops at intermediate steps, such as tetramer, unit-length filament, filament elongation, or IF maturation (17).

Thus, desmin assembly and/or desmin aggregation seem to depend on sequence, without obvious links to mutation position. Moreover, some post-translational modifications (PTMs) of desmin or other IFs have been linked to assembly/disassembly (17). Modifications of PTMs pattern have also recently been highlighted in myofibrillar (19,20) or cardiac pathology (21) context.

In addition, mouse *Des*$^{-/-}$ muscle cell mitochondria exhibit an increase in size and number, loss of correct positioning, and pronounced degeneration after work overload (22,23). Further, desL345P transgenic (24) or desR349P knock-in (KI) mice also present mitochondria mislocalization or enzyme dysfunction (25). These alterations indicate a link between oxidative metabolism and desmin.

Skeletal muscle fiber metabolism constantly generates reactive oxygen species (ROS) witch level depending to exercise intensity and regularity (26). Redox homeostasis continually neutralizes ROS with antioxidant protective molecules that belong to three main types: enzymes that can metabolize ROS and environmental oxygen peroxide (H_2O_2), endogenous non-enzymatic compounds, and exogenous non-enzymatic compounds (e.g., provided by food). Among endogenous antioxidants, glutathione appears to be most important in the context of muscular fatigue—the ratio between oxidized glutathione [disulfide glutathione (GSSG)] and reduced glutathione (GSH) is an indicator of redox status in cells or tissues (27). Among exogenous antioxidants, N-acetyl-L-cysteine (NAC) is known to counteract the increased levels of ROS and then to provide effects within muscle cells. In fact, this precursor of endogenous antioxidant, increases levels of the reduced glutathione before, during, and after exercise (28).

Imbalanced redox homeostasis is a pathogenic mechanism and thus potential therapeutic target in myopathies. Indeed, SEPN1-related myopathy, RYR1-related myopathy, or Duchenne muscular dystrophy have direct defects in redox regulation systems or have secondary redox abnormalities (29). Previously, pretreatment with NAC before H_2O_2 exposure significantly improved cell survival in SelN-devoid myoblasts, as well as in controls, whereas other food antioxidants did not (30).

Further, a link between oxidative stress and desmin protein aggregation has been shown in patient biopsies. Indeed, main glycoxidation marker (advanced glycation end product, N-carboxy-methyl-lysine, or N-carboxy-ethyl-lysine) levels are increased in muscle samples from individuals with desminopathies (31). Moreover, desmin is a major target of these oxidation and nitration modifications (32).

As patient cells are rarely available, we previously constructed isogenic cell lines expressing inducible wildtype (desWT) or mutant desmin—with mutations located in the head, rod, and tail domains (desS46Y, desD399Y, and desS460I, respectively)—to explore protein aggregation mechanisms. Only desD399Y is sensitive to stresses, such as heat shock or redox environmental changes (H_2O_2 or cadmium treatment). In addition, some antioxidant molecules, such as N-acetyl-L-cysteine (NAC) (33) and alpha-tocopherol (34), can prevent stress-induced aggregation.

Here, we first further expanded our inducible cell lines to other 2B mutations. Indeed, mutations in the end of the 2B domain of desmin are predominant (~66%) in human patients with desminopathies and lead to musculoskeletal and cardiac phenotypes of variable severity (35). This area also contains a stutter region, a conserved sequence important for filament assembly and stabilization (36). Thus, the 2B region seems essential for polymerization of the desmin network, perhaps making it susceptible to stress. Moreover A357P, Q389P, and R406W mutations share with D399Y a common skeletal muscle phenotype in patients (distal and proximal myopathy). Patients also mainly present respiratory insufficiency (except for Q389P) and cardiac defects (except for A357P) (for review see 17). R406W leads to the most severe phenotype and presents particular subsarcolemmal desmin accumulation in skeletal muscle.

Mutations introducing proline in the C-terminal part of the 2B domain are the most frequent (12 out of 24) (35). They lead to desmin aggregation and affect cellular assembly of IFs (37). However, not all mutations are dominant—A360P is recessive (13). We chosed to study at least two mutations carrying a proline: A357P and Q389P. These two mutations present a phenotype, especially on skeletal muscles, in agreement with our model of myoblasts. In addition to these two mutations, R406W substitution affects the YRKLLEGEE region, another extremely conserved and important domain in the regulation of network assembly (38–40).

Thus, we investigated whether the aggregative behaviors in stress conditions and the response to NAC pretreatment depend on the 2B location or on the specific mutation. Furthermore, we also analyzed the link between 2B mutations presenting stress induced aggregation and redox dynamics. To confirm the effect of NAC in a more physiological context, we performed experiments with injection of adeno-associated-virus (AAV), expressing WT or mutated desmin, in mouse tibialis anterior (TA) muscle, with or without antioxidant treatment. Finally, to understand these behaviors, we analyzed post-translational modifications (PTMs) of desmin in cell or in muscle. Indeed, as described for other intermediate filaments, some PTMs, such as phosphorylation, ubiquitination, sumoylation, glycosylation, and/or ADP ribosylation, are known to modify their behavior (41). Thus, they could also regulate desmin in response to stress.

Altogether, desmin cytoplasmic redox dynamic and PTMs alterations in our models provide new information on the variability and importance of oxidative redox balance in skeletal muscular cells containing a pathological variant of desmin.

Materials and methods:

Molecular model and secondary structure predictions

The crystal structure of human vimentin coil 2B fragment (CYS2) [residues 328 (Cys328)–411; PDB entry 1GK4] was used to construct desmin 2B end domain models (WT and mutant) with PYMOL software (DeLano Scientific LLC, Palo Alto, CA, United States). For energy minimization, computations were done in vacuo with GROMOS96 43B1 parameters set, without reaction field, from Swiss-PdbViewer 4.0.1 (http://spdbv.vitalit.ch/download.html). We used Pubmed Blast (http://blast.ncbi.nlm.nih.gov/Blast.cgi) for sequence alignment of CYS2 (residues 328–411) and desmin (residues 333–416).

Cell lines and culture

New stable cell lines from murine C2C12 myoblasts (ATCC, NY, USA) were generated as previously described (33). Briefly, mutagenesis was performed on pPuro-Myc-human-Desmin vector to introduce human mutations desA357P, desQ389P, and desR406W, following manufacturer's instructions (Quick Change-XL mutagenesis kit, Stratagene, San Diego, CA, United States). Plasmids were electroporated (Genepulser II, BioRad, Hercules,CA, United States; 500 µF, 350 V, with 10 µg of DNA) into clone 21 (tet-on) cells (33). Stable clones were selected after one week of puromycin selection. Doxycycline induction of human desmin variants was verified by western blotting (using c-Myc epitope antibody (1/1000, 9E10, Santa Cruz Biotechnologies, Dallas, TX, United States)) and immunostaining. Double stable cell lines were grown at 37°C and 5% CO_2 in Dulbecco's Modified Eagle's medium (DMEM, Life Technologies, Carlsbad, CA, United States) supplemented with 20%

fetal calf serum (Eurobio, Les Ulis, France), 1% penicillin/streptomycin (Life Technologies, Carlsbad, CA, United States), 1 mg/mL G418 (Euromedex, Souffelweyersheim, France), and 2 µg/mL puromycin (Euromedex, Souffelweyersheim, France).

Satellite cells were extracted from 2 gastrocnemius and 2 plantaris muscles of 1-month-old C56Bl6(N) knock-in mice for the R405W mutation (murine homologue of human desmin R406W; named after KI-R405W) (12). Following previous work (42), muscles were incubated 4 x 10 min in a solution of DMEM-10 HamF12/Glutamax (Life Technologies, Carlsbad, CA, United States) containing 1.5 mg/mL of protease XIV (Sigma-Aldrich, Saint-Louis, MO, United States) and 1/500 primocin (Invitrogen, Carlsbad, CA, United States) at 37°C under regular agitation. After each incubation, tubes were centrifuged at 400 g for 30 seconds at room temperature. Floating cells were eliminated, and 3 other fractions containing satellite cells were diluted in 20% FBS medium and sieved with a 40-µm filter. Filtrate containing satellite cells was centrifuged for 5 min at 1400 g at room temperature. Cells in DMEM-HamF12/Glutamax containing 20% FBS, 2% Ultroser (Pall Life Sciences, Portsmouth, United Kingdom), 8.6 ng/mL of FGF2 (Life Technologies, Carlsbad, CA, United States), 1/100 N2 (Life Technologies, Carlsbad, CA, United States), and 1/500 primocin were seeded onto 1/20 Matrigel-coated 6-well plates (Corning, Corning, NY, United States) at 1000 cells/well. After activation and proliferation, satellite cells were maintained or analyzed by seeding at 1000 cells/cm² on plastic covered with 1/20 Matrigel.

Oxidative and heat stress procedures

As previously described, stable cell lines were seeded at 3 x 10^3 cells/cm^2 in 6-well plates and induced with doxycycline (10 µg/mL, Sigma-Aldrich, Saint-Louis, MO, United States) after 24 h (28). Hydrogen peroxide and heat stresses were performed 48 h after induction as follows: 0.2 mM H_2O_2 (Sigma-Aldrich, Saint-Louis, MO, United States) was added to the cell culture for 2 h or cells were heat shocked at 42°C for 2 h. Cells were immediately analyzed (T0 time point) or media was replaced and cells were treated 24 h later (T24 time point). For pre-treatment, NAC (10 mM, #A7250 Sigma-Aldrich, Saint-Louis, MO, United States) was added to cells 16 h before stress.

Western blotting

Myoblast proteins were extracted by scraping cells in RIPA buffer without SDS [50 mM Tris pH 7.5, 150 mM NaCl, 5 mM EDTA, 1% NP40, 1 mM Na_3VO_4, 10 mM NaF, 1 mM PMSF, protease inhibitor cocktail 1X (complete mini, EDTA free, Roche, Bâle, Switzerland)] for 1D SDS-PAGE or urea buffer (8 M urea, 2 M thiourea, 4% CHAPS, 50 mM DTT) for 2D SDS-PAGE. After migration, proteins were transferred to nitrocellulose membranes (0.45 µm, Macherey Nagel, Düren, Germany), which were saturated with 5% non-fat milk in 0.5% Tween/PBS. Membranes were incubated with the primary antibody at the appropriate dilution for 1 h at room temperature or 16 h at 4°C. Primary antibodies used were: 1- mouse monoclonal anti-c-Myc (1/1000, 9E10, Santa Cruz Biotechnologies, Dallas, TX, United States); 2- rabbit polyclonal anti-desmin (1/1000, # C3956, Sigma-Aldrich, Saint-Louis, MO, United States); 3- mouse monoclonal anti-alpha-actin (1/2000, #MAB1501R, Millipore, Burlington, MA, United States); or 4- rabbit polyclonal anti-GFP (1/2500, A11122, Life Technologies, Carlsbad, CA, United States). Isotype-specific anti-mouse or anti-rabbit secondary

antibody coupled with horseradish peroxidase (1/10000, #31430 or #31460, Pierce, Thermo Scientific, Waltham, MA, United States) was detected by incubating with Clarity Western ECL (BioRad, Hercules, CA, United States) and visualized with a CCD camera (FUJI Las 4000 or Ai600, GE Healthcare, Chicago, IL, United States).

Cell immunofluorescence

Cells were fixed with 2% paraformaldehyde (Santa Cruz Biotechnologies, Dallas, TX, United States) for 15 min at room temperature, permeabilized 5 min with 0.5% Triton X-100, and incubated with mouse monoclonal anti-c-Myc primary antibody (1/100, 9E10 #sc40 Santa Cruz, Biotechnologies, Dallas, TX, United States) for 1 h at room temperature. After 3 washes with PBS, cells were incubated 45 min with isotype-specific anti-mouse secondary antibody labeled with Alexa-488 (#A11001, Molecular Probes, Eugene, OR, United States). DNA was stained with Hoechst 33258 (1 µg/mL, Sigma-Aldrich, Saint-Louis, MO, United States) for 10 min. Finally, cells were washed in PBS and mounted in Fluoromount medium (Interchim, San Diego, CA, United States). Images were acquired with confocal microscopy (LSM700 Zeiss, Iena, Germany) at the imaging facility of the Functional and Adaptive Biology (BFA) unit.

For aggregation measurements, images were taken as 5x5 tile scans on 3 random nuclear fields chosen in Hoechst-stained areas. Total cell number was calculated by counting nuclei with an ImageJ software in-house macro. Cells with aggregates were visually counted on the images. Aggregation percentage and ratio between stressed versus unstressed aggregated cells were calculated. Experiment was repeated at least 3 times.

Redox dynamics

Mammalian cell vector expressing cytoplasm-targeted HyPer (cyto-HyPer) was constructed by amplifying HyPer sequence (Evrogen, Moscow, Russia, (43)) and introducing a Nuclear Export Signal (NES). The PCR product, fusing NES in frame to the 3' end of HyPer, was then cloned in pCMV/myc/cyto vector (Life Technologies, Carlsbad, CA, United States). Vector expressing cytoplasm-targeted Grx1-roGFP2 (cyto-Grx1-roGFP2) was constructed in a similar way using pEIGW-Grx1-roGFP2 (Addgene, Cambridge, MA, United States (44)) as template. Expression vector encoding HyPer targeted to mitochondrial matrix (mito-HyPer) was purchased from Evrogen (Moscow, Russia). Stable cell lines or satellite cells were seeded at 11,500 cells/cm^2 or 22,000 cells/cm^2, respectively, in 6-well plates. After 24 h, cells were transfected with cyto-HyPer, mito-HyPer, or cyto-Grx1-roGFP2 in DMEM medium without antibiotics using JetPRIME (Polyplus-transfection, Illkirch-Graffenstaden, France) according to manufacturer's instructions. Eight hours after transfection, antibiotics were added, including doxycycline for desmin induction. Transfection efficiency was evaluated on an inverted fluorescence microscope with a FITC filter (Zeiss, Iena, Germany) at the imaging facility of the BFA unit.

Oxidative kinetics were started by adding 0.1 mM H_2O_2 to cells in complete media and incubating for 5, 15, 30, 60, or 120 min. Medium was aspirated and cells were washed with PBS and then overlaid with 15% trichloroacetic acid. After 30 min, cells were scraped and pelleted in 1.5-mL microtubes. After two washes with ice-cold acetone and air drying, pellets were resuspended in TES buffer (100 mM Tris pH 8.8, 10 mM EDTA, 1% SDS). Loading buffer without reducing agent was added to samples. Equal volumes were loaded on 12% SDS acrylamide gels and results were analyzed by western blotting.

Intramuscular injection of AAV vectors

Plasmids encoding c-Myc-tagged human desmin (desWT and desD399Y) under the regulation of the CMV promoter were used to prepare AAV vectors. AAV2/2.CMV.Myc-desWT (AAV-desWT) or Myc-desD399Y (AAV-desD399Y) were provided by the Vector Production Center of the Therapeutic Research Institute at the Health Research Institute of the University of Nantes (UMR1089, Nantes, France). Final viral preparations were split in 50-µL aliquots in D-PBS (with Ca^{2+} and Mg^{2+}) and stored at −80°C. Number of viral genomes (vg) was titrated by polyA quantitative PCR and was 5.2 x 10^{12}.mL^{-1} for AAV-desWT and 5 x 10^{12}.mL^{-1} for AAV-desD399Y.

The injection procedure was previously described by Joanne et al. (45) Briefly, for intramuscular injections, 11 week-old male C57BL/6J mice (Janvier Labs, Le Genest-Saint-Isle, France) were anesthetized by intraperitoneal injection of an analgesic and sedative drug mix [100 $mg.kg^{-1}$ ketamine (Merial, Lyon, France) and 10 mg/kg xylazine (Bayer, Leverkusen, Germany)]. Each TA muscle was injected with 70 µL of AAV diluted in PBS (~3 x 10^{11} vg/70 µL) using an insulin syringe. Animals were split into 4 groups of n=5 mice: AAV-desWT with NAC, AAV-desWT without NAC, AAV-desD399Y with NAC, and AAV-desD399Y without NAC. NAC was diluted to 20 mM in drinking water. Bottles were changed every 2–3 days and weighed before and after replacement to calculate the absorption volume of NAC by mice.

Animal experiments were conducted with respect to animal health and well-being, and all procedures were approved by our institutional ethics committee (authorization APAFIS#5441 -20 16052314036983 v7, for AAV-injected mice; CEB-16-2016, for KI-R405 mice). All procedures were also conducted according to French and European

laws, directives, and regulations on animal care (European Commission Directive 86/609/EEC; APAFIS#5441 -20 16052314036983 v7). For AAV experiments, the animal facility (Centre d'expérimentation Fonctionnelle (CEF), Pitié Salpétrière Hospital, Paris) is fully licensed by French competent authorities and has animal welfare insurance.

Preparation of TA muscles

TA muscles were removed 1 or 2 months following injection after euthanizing mice by cervical dislocation. For immunohistochemical analysis, muscles were embedded in tragacanth gum (Fisher Scientific, Hampton, NH, United States) and frozen by plunging in isopentane precooled in liquid nitrogen for at least 1 minute. For western blotting, muscles were directly frozen in liquid nitrogen in microtubes and later pulverized in a cryogenic mortar (Dutscher, Issy-les-Moulineaux, France) and resuspended in urea buffer for 2D gels.

Muscle sections and histological staining

Serial sections of 6 µm thickness were sliced using a CM1950 cryostat, (Leica, Wetzlar, Germany) recovered on Superfrost Plus microscope slides (Thermo Scientific, Waltham, MA, United States), and stored at –80°C. Muscle sections were kept at room temperature for 20 min before staining with either hematoxylin/eosin (HE), succinate dehydrogenase (SDH), or fluorescent antibodies as follows.

HE: Transverse muscle sections were incubated with 0.7% hematoxylin solution (Harris modified, Sigma-Aldrich, Saint-Louis, MO, United States) for 6 min at room temperature, washed 5X with water, and stained with 0.5% eosin in acidified 90% ethanol (Sigma-Aldrich, Saint-Louis, MO, United States) for 1 min at room

335 temperature. Muscle sections were dehydrated by incubating in successive baths of
336 gradually increasing ethanol concentrations (30%, 50%, 70%, 85%, 95%, and 100%,
337 repeated twice) for 2 min each, followed by two baths in clearing solution (Histo-
338 Clear, National Diagnostics, Atlanta, GA, United States) for 10 min and 15 min, and
339 rapidly mounted in VectaMount medium (Clinisciences, Nanterre, France). Images
340 were acquired on a stereomicroscope (Leica, Wetzlar, Germany) at the BFA unit.

341 SDH: Transverse muscle sections were stained by immersion in SDH buffer (0.2 M
342 phosphate buffer containing 5.4% sodium succinate and 0.1% nitro blue tetrazolium)
343 for 2 h at 37°C and then washed with water. Finally, muscle sections were either
344 mounted directly in VectaMount medium (Clinisciences, Nanterre, France) or
345 processed for further immunofluorescence. Images were captured on a
346 stereomicroscope (Leica, Wetzlar, Germany) at the BFA unit.

347 Immunostaining: Warmed muscle sections were fixed with 4% paraformaldehyde for
348 10 min at room temperature. Endogenous fluorescence was prevented with 50 mM
349 NH_4Cl for 30 min. Sections were permeabilized in 0.5% triton/PBS for 10 min,
350 blocked in 1% bovine serum albumin/PBS, and incubated with rabbit anti-Myc
351 (1/1000, # C3956, Sigma-Aldrich, Saint-Louis, MO, United States) or rabbit anti-
352 laminin (1/100, #L9393, Sigma-Aldrich, Saint-Louis, MO, United States) primary
353 antibodies for 1 h at room temperature or overnight at 4°C. Primary antibodies were
354 detected by incubating sections with suitable secondary antibodies for 45 min.

355 DNA was stained with 1 $\mu g.mL^{-1}$ Hoechst 33258 (Sigma-Aldrich, Saint-Louis, MO,
356 United States) for 10 min. Cells were washed in PBS and mounted in Fluoromount
357 medium (Interchim, San Diego, CA, United States). All images were captured using a

digital camera mounted to a confocal laser scanning microscope (LSM700 Zeiss, Iena, Germany) at the imaging facility of the BFA unit.

Analysis of TA muscle characteristics

TA fiber amount and diameter (minimum Feret values) were calculated on whole muscle transverse sections stained with laminin. Images were analyzed with ImageJ software. Percent transduction was calculated by measuring the number of fibers that were positively stained for Myc compared to the total number of fibers in the section. For aggregation rate, number of fibers containing aggregates was reported in relation to total transduced fibers.

2D gel electrophoresis

2D gel electrophoresis was performed at the proteomics platform at the Cochin Institute (Paris, France). Briefly, protein separation was performed by isoelectrofocusing on 7-cm pH 4–7 strips in the first dimension and SDS-PAGE on 10 or 12% polyacrylamide gels in the second dimension. Proteins were transferred to nitrocellulose membranes and analyzed by western blotting. Calculation of theoretical isoelectric points (pI) for Myc-labeled desWT and mutant desmin proteins provided different values according to the website used (Table 1).

Isoelectric point (pI) calculation	**ExPASy**	**Protein Calculator v3.4**	**Protein isoelectric point calculator**	**Scansite**
WT murine desmin	5.21	5.28	5.05	5.21
WT human desmin	5.21	5.28	5.06	5.21
WT Myc-desmin	5.11	5.17	5.07	5.11
D399Y Myc-desmin	5.15	5.20	5.03	5.15

Table 1: Algorithmic isoelectric point (pI) calculations from different web sites:
ExPASy (https://web.expasy.org/compute_pi); Protein Calculator v3.4 (http://protcalc.sourceforge.net);
Protein isoelectric point calculator (http://isoelectric.org);
Scansite (https://scansite4.mit.edu/4.0/#calcMolWeight).

One site also indicates phosphorylated peptide molecular weights and phosphorylation that regulate desmin network assembly. For tagged desWT, the obtained values are detailed in Table 2.

Phosphates	**0**	**1**	**2**	**3**	**4**	**5**	**6**	**7**	**8**
Molecular weight (kD)	54.7	54.8	54.9	54.9	55.0	55.1	55.2	55.3	55.3
Isoelectric point	5.11	5.07	5.04	5.00	4.97	4.94	4.91	4.88	4.85

Table 2: Predictions of molecular weight evolutions and isoelectric points according to the number of phosphorylation of desWT (https://scansite4.mit.edu/4.0/#calcMolWeight).

Statistical analysis

Box plots were created with GraphPadPrism software or R free software, and results were statistically analyzed with non-parametric tests—“nparcomp” function with

Dunnet comparison to WT, or Tukey comparison for others. Curves, scatter plots, and histograms as well as corresponding graphic analyses were done with GraphPadPrism software—either 2-way ANOVA corrected by Bonferroni non-parametric function, or Kruskall-Wallis tests. Significant differences were considered at $p < 0.05$.

Results:

DesA357P, desQ389P, desD399Y, and desR406W mutants located in the 2B desmin rod domain exhibit *in silico* distinctive structural interactions.

DesD399Y is located distally in the 2B desmin rod domain. We previously demonstrated that it exhibits stress-induced aggregation, whereas mutations located in the head (desS46Y) or tail (desS460I) do not display this aggregation (33). To further investigate mechanisms leading to stress-induced aggregation, we chose three other pathological mutations—desA357P, desQ389P, and desR406W (Figure 1A)—also located in the end of this domain between stutter and C-terminal regions, which is a notorious mutation hot spot (35).

First, we constructed desmin 2B end domain mutant and WT models with PYMOL software and compared *in silico* the impact of each substitution (Figure 1B). A357P is located in the stutter region that is considered critically important for proper filament assembly. Further, it is in the "e" position in the heptad (internal residue repeats conserved in IF, as described by Strelkov et al.(46). On our structural representation, it is well inside the dimer and phenylalanine lateral chains face in both directions. We can see the position of alanine in the helix/dimer and its replacement with proline. Representation of structural modifications occurring with Q389P substitution shows

loss of a large negative side chain residue and gain of a small neutral one. D399Y and R406W substitutions provide insight about ionic bridging over two disrupted domains—in both, ionic residues are replaced with aromatic amino acids.

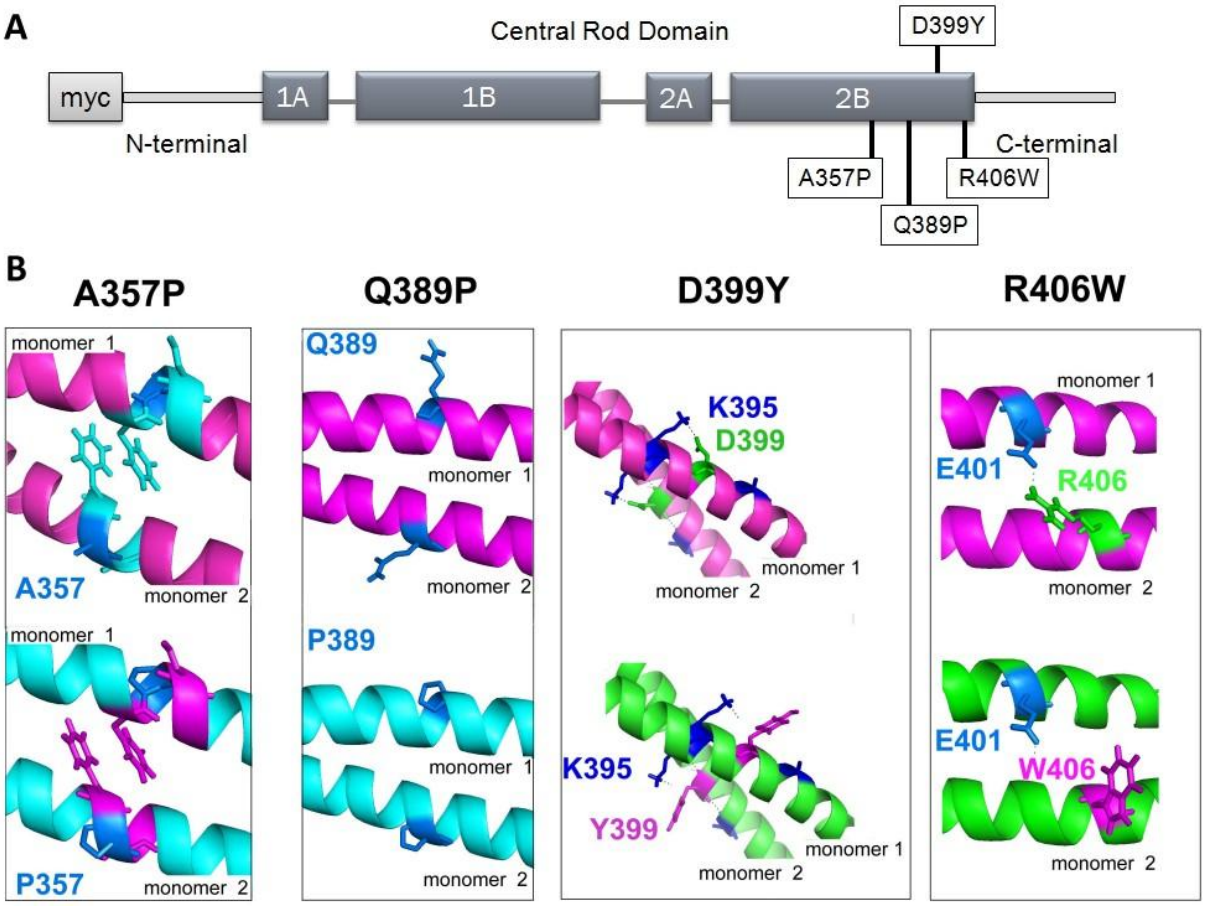

Figure 1: Mutation locations within desmin structure and in silico modeling of mutation effects on structure of desmin coiled coil 2B domain. (A) Overview of desmin structure showing locations of individual mutations in the 2B domain and myc tag. (B) Graphic representation of tripartite desmin, based on vimentin crystal structure (1gk4), with mutations in central rod 2B domain of each monomer, with amino acids of interest represented by molecular structures. WT helical regions are magenta and mutants are cyan or green. A357P and Q389P mutations are dark blue. A357P is located in the stutter region, so conserved phenylalanine is also in molecular structure. D399 and R406 interactions (salt-bridge) with side chain residue K395 or E401 are in dark blue and are represented with dotted lines.

New stable cell lines expressing desmin mutations exhibit the same expression level as desD399Y-expressing cells.

Second, we generated six new inducible stable cell lines (2 clones per mutation) expressing desA357P, desQ389P, and desR406W according to the same protocol that we used for desD399Y and desWT (25). Expression in all clones was analyzed by western blot to confirm the level of exogenous human desmin compared to desD399Y (Figure 2).

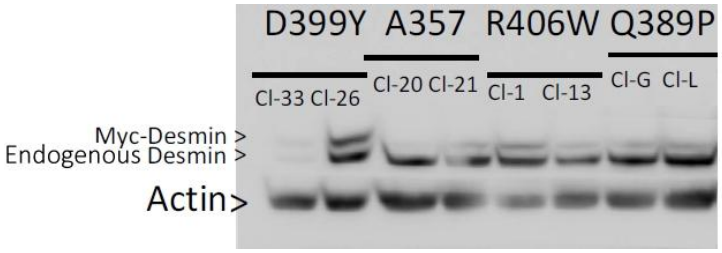

Figure 2: Steady-state desmin expression levels. Western blot of endogenous and human Myc-desmin in inducible stable cell lines 72 h after induction (T24 without stress). Actin represents a loading control. "Cl-*X*" represents name of the selected clone for each desmin mutation.

For each mutation, one construct expressed low levels of desmin and another expressed higher levels. At steady state, endogenous desmin was always more highly expressed than exogenous protein (maximum ratio exogenous/endogenous of 1:1 for desWT clone 29 and 0.8:1 for des D399Y clone 26; Table 3). Overall, clones had a similar ratio of ~0.4:1, permitting us to compare new inducible clones to each other in basal conditions or upon stress. Moreover, as demonstrated in table 3, the basal protein aggregation in these cells remained below 3.5% (Table 3).

Clone	Desmin expression ratio (exogenous/endogenous)	Basal aggregation (%)
desWT-Cl-16	0.4	0.6
desWT-Cl-29	1.0	
desD399Y-Cl-26	0.8	2.9
desD399Y-Cl-33	0.8	2.1
desA357P-Cl-20	0.1	0.5
desA357P-Cl-21	0.3	
desR406W-Cl-1	0.5	1.4
desR406W-Cl-13	0.4	3.5
desQ389P-Cl-G	0.2	2.0
desQ389P-Cl-L	0.3	3.0

Table 3: Steady-state desmin expression levels and aggregation percentages. Western blot analysis of endogenous and human Myc-desmin in inducible stable cell lines 72 h (T24) after induction. Quantification was realized with ImageJ software. Protein amounts were normalized with anti-alpha-actin antibody (Actin). Basal aggregation percentage was calculated as described in material and methods.

Stresses induce protein aggregation only in desQ389P, desD399Y, and desR406W, with varying aggregate morphologies.

We measured desmin aggregation in all stable cell lines in response to oxidative or heat shock stresses after 24h. In response to stress, a normal desmin network was present in desWT- or desA357P-expressing cell lines (Figure 3A, first row).

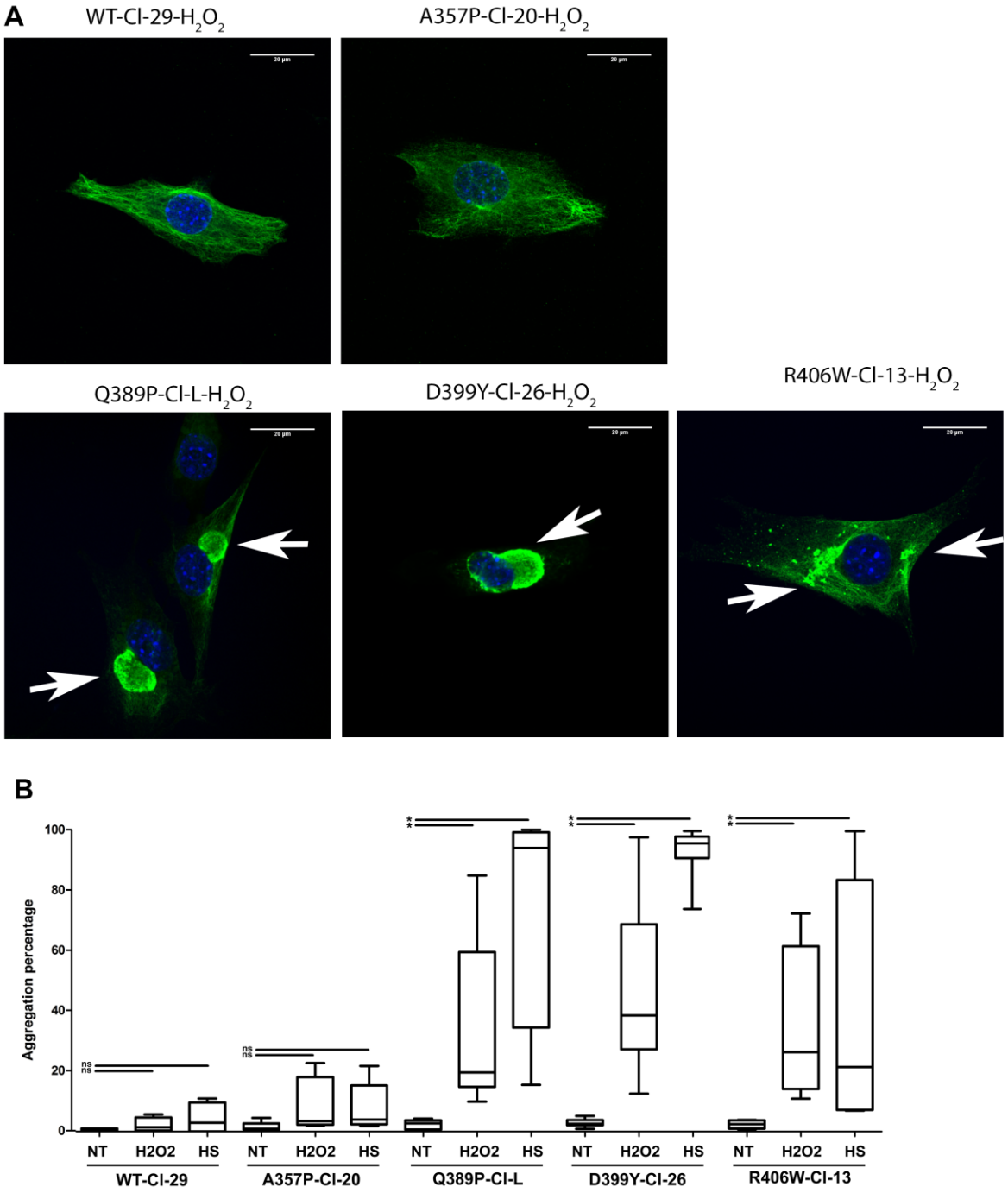

458

459 **Figure 3: Increased aggregation upon stresses in desD399Y, desQ389P, and R406W cells, but**
460 **not desA357P cells**. (A) Representative confocal micrographs showing immunostaining at 24 h after
461 oxidative stress (T24) for Myc-desmin (green) and Hoechst dye (blue). DesWT and desA357P form
462 normal networks. DesQ389- and desD399Y-expressing cells form large aggregates near the nucleus
463 (arrows, left and middle panels). DesR406W-expressing cells form smaller accumulations distributed
464 throughout the cytoplasm (arrows, right panel). White bar = 20 µm, 40x magnification. (B) Box plot
465 representing the aggregation percentages 24 h after stress (T24) compared to untreated cells. Three
466 different treatments are shown: heat shock (HS), oxidative stress (H_2O_2), and no stress (NT). Cells
467 were counted in at least 3 independent experiments (>100 cells each) (ns: not significant; *p < 0.05,
468 compared to unstressed).

As previously described, stress of desD399Y-expressing cells induced large aggregates very close to the nucleus (Figure 3A, middle in second row). DesQ389P displayed similar characteristics (Figure 3A, left in second row). DesR406W also exhibited stress-induced, variably-shaped aggregates, although they had weaker staining, maybe due to small size. These aggregates were also more numerous and more dispersed in the cytoplasm (Figure 3A, right in second row). We quantified aggregation rates for each stable clone, representing cells with any aggregates, as compared to the total cell population (Figure 3B, Supp. Data 1). DesA357P-expressing cells presented the same pattern as desWT, with no modification of aggregation rate, indicating that desA357P cells are not sensitive to oxidative or heat shock stress. In contrast, heat shock significantly induced a high aggregation rate for desQ389P and desD399Y (~20–40-fold increase), while oxidative stress led to significant, but less, aggregation (~10-fold increase). DesR406W cells also had significant aggregation in response to stress, although with more dispersed values. The anti-aggregative effect of NAC in the oxidative condition was confirmed for desQ389P, desD399Y, and desR406W (Figure 4). Indeed, ratios of aggregate percentages comparing NAC-treated and untreated cells showed a noticeable decrease. For all cell lines sensitive to oxidative stress, NAC pretreatment significantly reduced stress-induced aggregation.

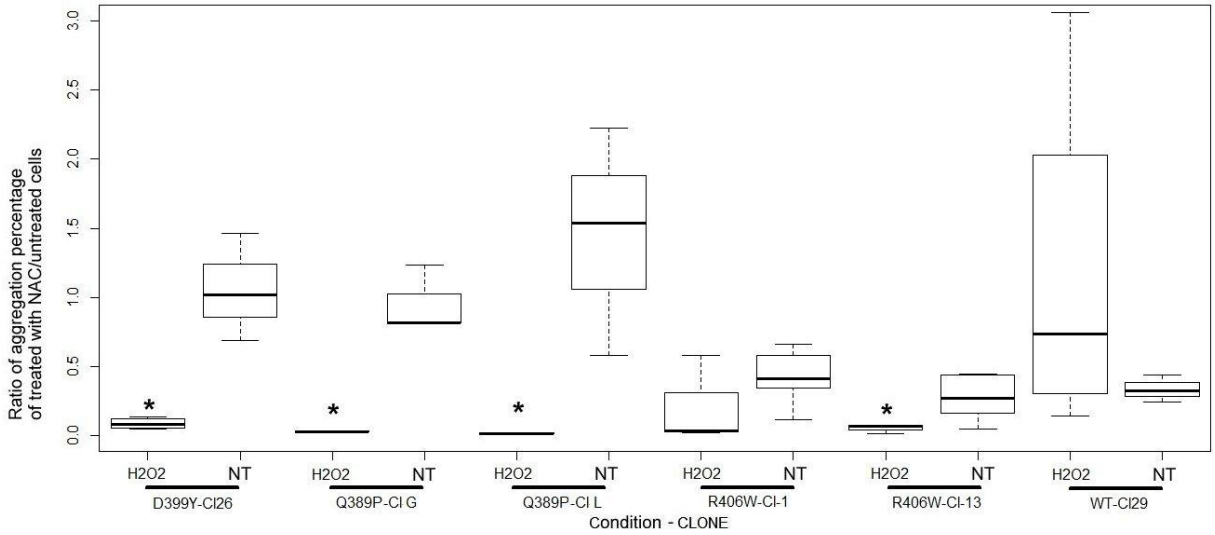

Figure 4: Effect of NAC as an anti-aggregative molecule on stable cell lines expressing desQ389P, desD399Y, and desR406W. First, aggregate-containing cells were quantified, untreated or pretreated with NAC, 24 h after stress or control conditions (NT). Then, box plots represent the ratio of percentage of cells with aggregates in the presence of NAC, reported to untreated cells. Cell counting was performed on three independent experiments (~100 cells each). For each clone, compared to its control NT, $*p < 0.05$, as calculated with Kruskall-Wallis non-parametric test.

Cytoplasmic redox dynamic in desmin mutant cell lines exhibits various behaviors.

To further investigate how stress induces aggregation in all responsive cell lines and how NAC can prevent this effect, specific redox reporters were used to monitor redox balance in cells expressing desmin mutants following oxidative stress. We first used the cyto-Grx1-roGFP2 to monitor cytoplasmic redox dynamic. This reporter specifically reacts with GSSG/GSH in the targeted compartment, so the percentage of the oxidized form reflects the redox state of glutathione (44) (Figure 5A and 5B). A second probe, HyPer, reacts specifically with H_2O_2 and is targeted to the cytoplasm (cyto-HyPer). Therefore, the percentage of the oxidized form of cyto-HyPer reflects the quantity of cytoplasmic H_2O_2 over time (Figure 5C and 5D).

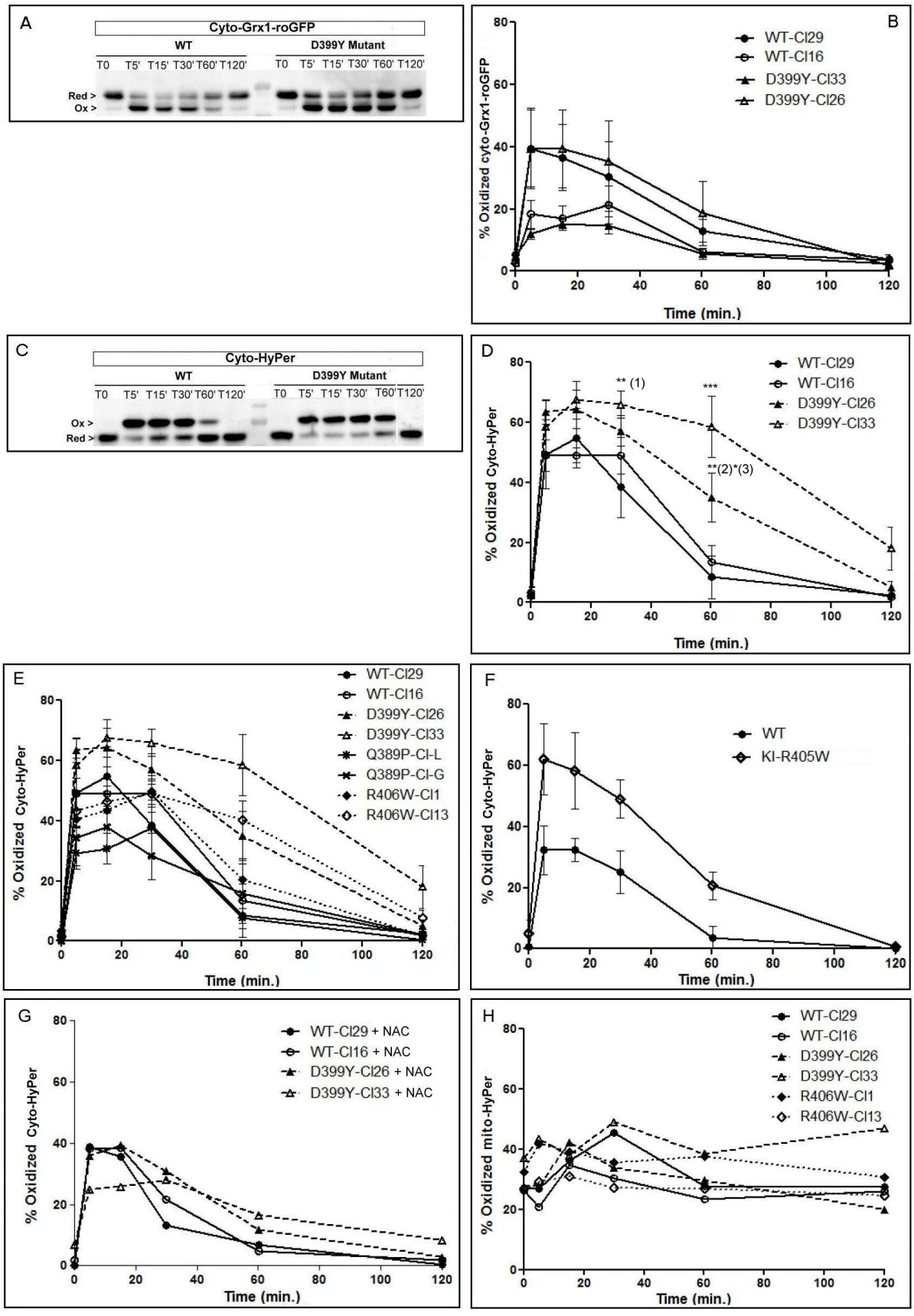

506

507 **Figure 5: desD399Y and desR406W trigger alteration of redox balance during stress.**

(A) Representative western blots of the oxidized and reduced forms of cyto-Grx1-roGFP2 reporter following oxidative stress in stable cell lines expressing desWT or desD399Y (B) Quantification of oxidation kinetics of the cyto-Grx1-roGFP reporter over time. (C) Representative western blots of the oxidized and reduced forms of cyto-HyPer reporter following oxidative stress in stable cell lines expressing desWT or desD399Y with the cyto-HyPer reporter. (D) Quantification of oxidation kinetics of the cyto-HyPer reporter over time. (E) Percentage of oxidized cyto-HyPer in stable cell lines expressing desWT, desD399Y, desQ389P, or desR406W, without pretreatment. (F) Percentage of oxidized cyto-HyPer in satellite cells from KI-R405W mice. (G) Percentage of oxidized cyto-HyPer in stable cell lines expressing desWT or desD399Y after NAC pretreatment (10 mM). (H) Percentage of oxidized mito-HyPer in stable cell lines expressing desWT, desD399Y, desQ389P, or desR406W, without pretreatment. Each point represents the mean of three independent experiments, with bars indicating SEM. Prism software was used for 2-way ANOVA, corrected by Bonferroni non-parametric function (*$p < 0.05$; **$p < 0.01$; ***$p < 0.001$).

Both cyto-Grx1-roGFP2 and cyto-HyPer probes were first compared in experiments with desWT and desD399Y clones. There were no significant differences in cells expressing desWT or desD399Y with Cyto-Grx1-roGFP (Figure 5B). Using cyto-HyPer, however, we detected significantly delayed oxidation kinetics in the cytoplasm of desD399Y clones (Figure 5D). Indeed, more H_2O_2 remained in desD399Y clones at 60 min after the beginning of oxidative stress compared to desWT clones, although both constructs reached near-zero values after 120 min.

We thus expanded cyto-HyPer probes analysis to the two other mutants with stress-induced aggregation, desR406W and desQ389P. Similar to desD399Y, both clones expressing desR406W had similar significant differences in reporter oxidation depending on the duration of oxidative stress (Figure 5E). We confirmed these results using the more physiological model of satellite cells extracted from our new KI-R405W animal model. These cells showed very comparable delayed recovery of basal reporter reduction (Figure 5F). In contrast, unexpectedly considering the aggregative pattern seen in Figure 3A, desQ389P cell lines have a similar behavior to desWT (Figure 5E).

To better understand the effect of NAC pretreatment on the evolution of cytoplasmic content during H_2O_2 incubation, we made the same measurements in the presence

of NAC. NAC especially reduced the percentage of oxidized reporter in cells expressing desD399Y (Figure 5G). Differences in the averages between untreated and treated showed that this decrease was ~16%–25% for both.

Finally, we investigated the mitochondrial effect of H2O2 incubation using the mitochondrial matrix-targeted HyPer reporter. Redox balance is distinct in this organelle, as the reporter was more oxidized even without treatment and remained unchanged in all experiment conditions (Figure 5H). This indicates that mitochondria are not affected as cytoplasm in response to oxidation.

Expression of desD399Y *in vivo* induces aggregation with slightly altered SDH repartition in adult mouse muscle fibers.

Heat-shock and oxidative stress are two types of environmental variations that can be found in muscle physiology (47). DesD399Y induces aggregation following these environmental stresses, as do other mutations, such as desQ389P or desR406W. We used a specific desD399Y mouse model with AAV-injected TA muscle to confirm the anti-aggregative effect of NAC *in vivo*. We initially injected AAV containing desWT or desD399Y in TA muscle of C57BL/6J mice and then analyzed resulting desmin expression and aggregation with or without NAC treatment after 1–2 months.

We calculated transduction efficiency by counting anti-Myc-stained fibers compared to all fibers stained with laminin (Figure 6A and B). Surprisingly, transduction efficiency was variable and higher for desWT (mean: 75%) than desD399Y (~50%), regardless of the duration before analysis (1 or 2 months).

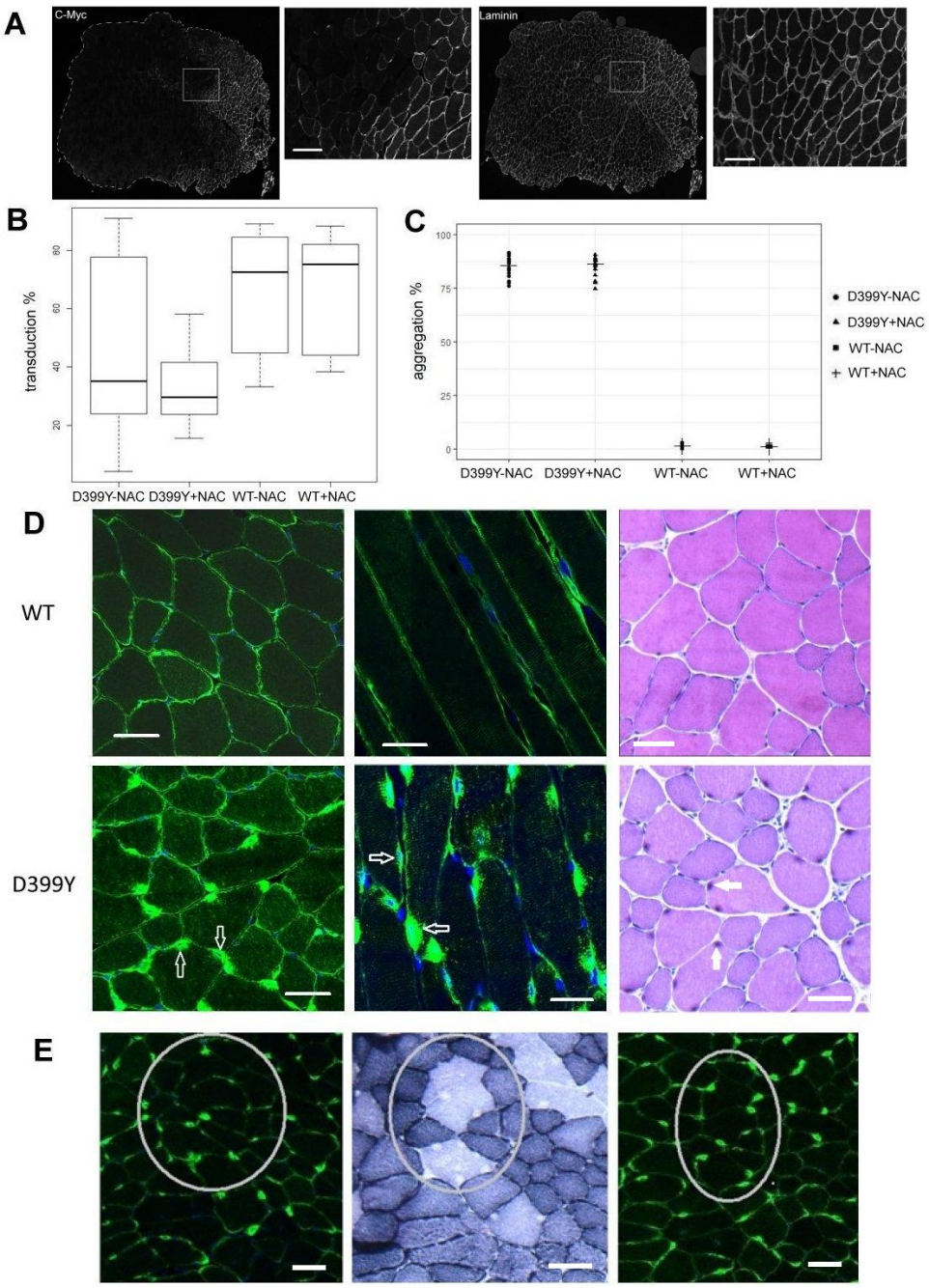

Figure 6: AAV-injected muscles overexpressing desD399Y mimic some important features of human desminopathies: an *in vivo* model to test the effect of NAC as a putative anti-aggregative molecule. (A) Representative images of immunohistochemical staining of muscle cross-sections with anti-Myc antibodies to visualize transduced fibers (left) and laminin to visualize all fibers (right). Results are quantified in plots of (B) transduction percentage and (C) aggregation percentage from 4 injected mouse TA muscles for each condition. (D) Confocal micrographs of transversal (left) and longitudinal (middle) sections of muscle expressing desWT or desD399Y stained with anti-Myc antibodies (green). Nuclei are counterstained with Hoechst dye (blue). Right panels show HE-stained transverse sections imaged with a stereomicroscope. White arrows indicate aggregates. Images taken with a 40x objective; white bar = 25 µm. (E) Confocal micrographs of a series of desD399Y-injected muscle cross-sections stained with anti-Myc antibodies (green) and Hoechst dye (blue) (left and right panels) or SDH (middle panel). Circles highlight area with aggregation and the absence of SDH staining. Images taken with a 40x objective.

As expected, expression of ectopic desmin was detected in muscle protein extracts after western blotting with anti-Myc or anti-desmin antibodies (Supp. Data 2). Aggregation percentages were evaluated by counting fibers with aggregates, regardless of the number of aggregates, compared to all fibers (Figure 6C). In AAV-desWT-injected TA, <5% of fibers presented aggregates, while ~95% of AAV-desD399Y-injected fibers were positive for aggregates. As observed in stable cell lines, aggregates were always localized around nuclei (Figure 6D). Disorganization of surrounding z-disks, as observed in patient biopsies with aggregates, was not noted. In a few cases, fibers with aggregates had some areas without SDH staining (in circles in Figure 6E). Those small spots indicated absence of enzyme activity and were smaller than rubbed-out fibers observed in patient biopsies (i.e. where, in some muscle fibers, SDH stain looks as though it has been rubbed away inside the fiber). In addition, we quantified fiber size in injected muscles. Minimum Feret diameters (min Feret) is commonly considered a better marker than area measurement for muscle physiology comparisons, because it minimizes the effects of oblique sectioning. AAV-desD399Y-injected muscles have slightly decreased min Feret diameter of fibers compared to AAV-desWT-injected muscles (Supp. Data 3). Altogether, data indicate that AAV-desD399Y injected muscle mimics some main human desminopathy features and could serve as a model to test the antioxidative effects of NAC.

The day following injection, we split mice into two groups: one with untreated drinking water, and one with 20 mM of NAC solution in the drinking water. Despite results with cell lines expressing desD399Y, aggregation was similar with or without NAC treatment (Figure 6C). However, unexpectedly and independently of the desD399Y

599 mutant, NAC treatment increased the total number of fibers (Supp. Data 3A) and
600 seemed to be associated with a slight decrease in min Feret diameter (Supp. Data
601 3B).

602 **2B desmin mutants exhibit different PTM patterns *in vitro* and *in vivo*.**

603 To understand some molecular alterations of desminopathies upon stress, we
604 investigated PTMs in our cell and mouse models of pathological mutations under
605 different environmental factors. We hypothesized that PTM differences can be linked
606 to stress-induced aggregation, as highlighted previously. We thus used bidirectional
607 gels to look for differences between exogenous desmin PTMs in stable clones
608 expressing desWT versus mutants 24 h after heat shock or oxidative stress, or in
609 injected muscles.

610 As expected, human Myc-tagged desmin presented a pI of ~5.2 (coherent with Table
611 1). However, we observed several patterns. Untreated desWT cells (clone 29) had
612 four spots, whereas heat-shocked cells had at least eight spots with the same
613 molecular weight (Figure 7, first line, two first columns). DesD399Y cells showed the
614 same pattern, although they presented several additional spots with higher molecular
615 weights (Figure 7, second line, two first columns). We found similar results after
616 oxidative stress by H_2O_2 (Figure 7, fourth column), although treated desWT-
617 expressing clones did not have as many spots as expected (Figure 7, WT/H_2O_2 T24).

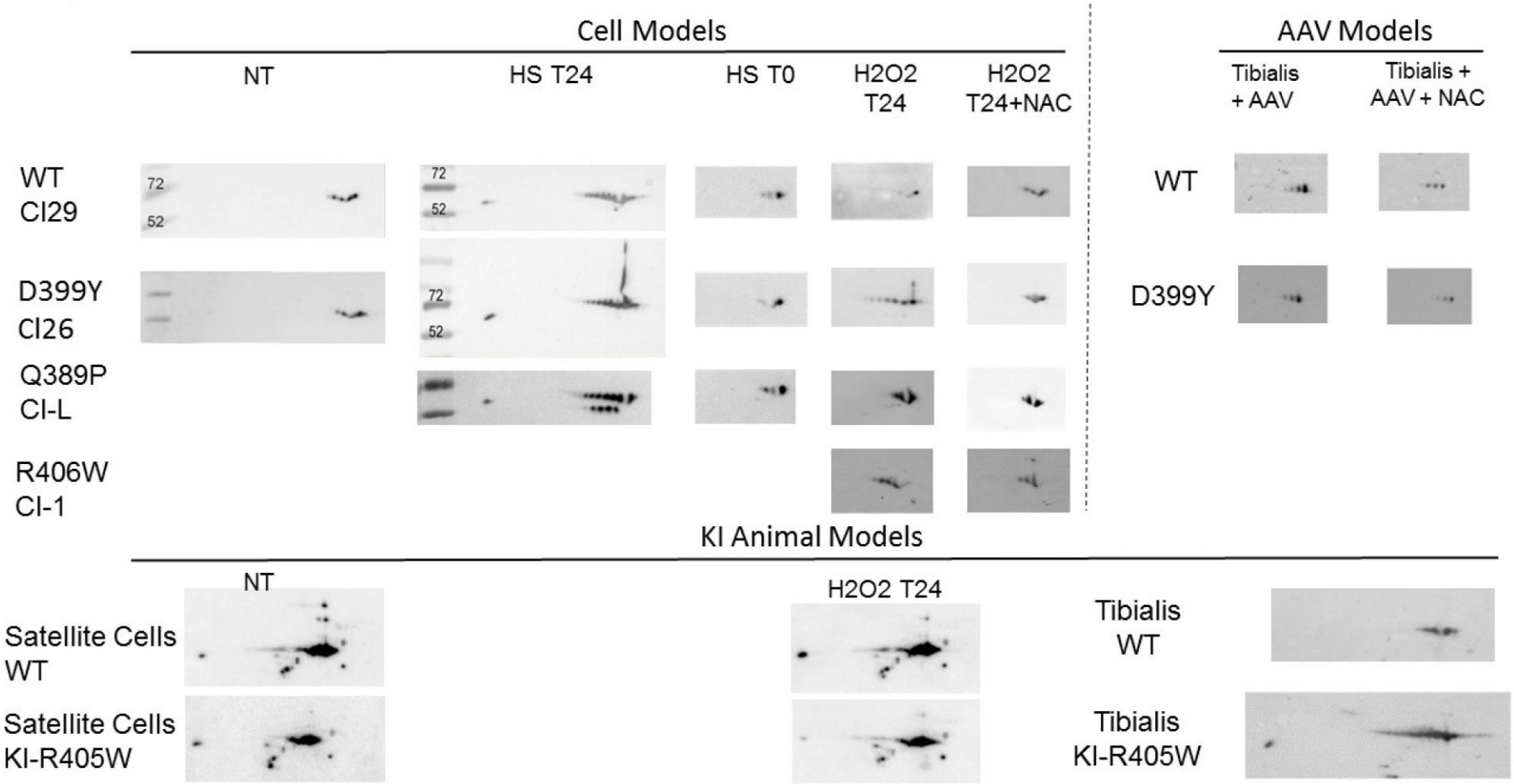
Cell Models
AAV Models
NT
HS T24
HS T0
H2O2 T24
H2O2 T24+NAC
Tibialis + AAV
Tibialis + AAV + NAC
WT CI29
D399Y CI26
Q389P CI-L
R406W CI-1
WT
D399Y
72
52
KI Animal Models
NT
H2O2 T24
Satellite Cells WT
Satellite Cells KI-R405W
Tibialis WT
Tibialis KI-R405W

618

Figure 7: Stress induces various desmin PTMs, depending on the mutation. For cell models (left): 2D-PAGE analysis of total protein extracts from stable clones expressing desWT (WT-Cl29) or mutant desD399Y (D399Y-Cl26), desQ389P (Q389P-Cl-L), or desR406W (R406W Cl-1) or satellite cells from KI-R405W mice. Samples represent different time points (T0, just after stress; T24, 24 h after stress) and stresses [thermal, HS, or oxidative (H_2O_2)] with or without NAC pretreatment. For muscles (right): 2D-PAGE analysis of total protein extracts of TA muscles, either AAV-injected (with desWT or desD399Y), treated with NAC for 2 months or untreated, or from KI-R405W mice.

After exposure to heat shock or oxidative stress, extracts from the stable clone expressing desQ389P presented two forms of desmin with close molecular weights (Figure 7, third line). One is the expected size of desmin (53 kDa) with several additional spots that could represent desD399Y, and the second is close to 49 kDa. The day after oxidative stress, desR406W also had a different migration profile from desWT. We observed four spots, with some additional lower-molecular-weight spots close to 49 kDa, similar to Q389P but with a higher pI (~5.4).

Because aggregates are already present 24 h after stress, we wanted to determine whether the observed PTMs take place just after the stress, when no aggregation is detectable. For all analyzed cell lines, desmin patterns at T0 were the same as for untreated cells (four spots) (Figure 7, third column). We also examined the patterns at T4h, when aggregation begins for the three previously studied cell lines (33). Profiles were similar to those obtained at T0—four spots of different pIs but similar molecular weights (data not shown). Thus, these results suggest that PTMs are probably a post-aggregative process.

We also analyzed desmin patterns by 2D-PAGE after stressing cells that were pretreated with NAC. Except for desR406W, all mutant patterns in the presence of NAC were similar to desWT without stress (Figure 7, fifth column). For desR406W, spots corresponding to potential proteolysis remained present, potentially with one additional higher-molecular-weight spot.

To further analyze our *in vivo* results, we compared these patterns to protein extracts from AAV-desWT-injected or AAV-des-D399Y-injected muscles. None of the modifications observed in cells could be detected in muscle given the high presence of aggregates and morphological alterations presented above (Figure 7, last two columns). Indeed, in AAV-desWT-injected as well as AAV-D399Y-injected muscles in the absence of NAC, four forms of desmin appeared at the expected molecular weights. After pretreatment with NAC, the profile appeared to be globally identical, although only three spots seemed to remain, with probable disappearance of the highest-pI form.

Finally, patterns obtained with muscles or satellite cells from KI-R405W (Figure 7, last lines) displayed many PTMs around the values in Tables 1 and 2, indicating both molecular weight and potential known phosphorylation modifications.

Discussion:

Usually, no proline residue is present in the central domain in desmin alpha helices. This residue is known to create a bend of ~25° in the helix (48). However, with Pymol software, it is only possible to visualize that the alpha amine of this residue no longer participates in alpha helix stabilization. Helix 2B length and rigidity may be sufficient to attenuate this deformation. In the case of replacement of alanine with a proline (A357P), this position supposedly stabilizes the dimer with ionic interactions. Substitution of proline at least alters the alpha helix and should be enough to drive the pathological phenotype. Size and bulkiness of the side chain has a moderate effect, as shown in Figure 2B, and affects hydrophobicity. Pymol software indicates that the helix deformation for Q389P comes with a moderate potential change outside the coiled coil, which can affect interactions between several dimers and may

impact polymerization. Proline extends less beyond the helix than glutamine, which may affect assembly of the dimers in tetramer and/or radial compaction. In fact, Q389P could be compared to other mutations leading to replacement of a residue by a proline, such as R350P (b in heptad as Q389P), A357P (e in heptad as D399Y), and L370P (inside the heptad, leading to a lost hydrophobic interaction). However, R350P is upstream of the stutter, A357P is in the stutter, and L370P creates a bend in a conserved sequence, similar to Q389P, but at different coiled coil locations. It is therefore possible that proline destabilization of the alpha helix is not equivalent for these four positions, even if their pathogenic effect is established (37). On the other hand, abolishing interactions between side chains [C–O of aspartate (399) or glutamate (401) with NH of lysine (395) or arginine (406)] may destabilize the dimer. In addition, tyrosine spreads much more than aspartate and changes the charge at this position. For tryptophan, its orientation and size are also very different from those of arginine. These two mutations could also interfere with dimer assembly in the tetramer and/or with radial compaction. For R406W, modeling has already been used to study the interactions of desmin and synemin (49), which strengthens the desmin network. These anchors are not permitted by the mutation, even though the 406 residue is not in charge of the interaction. Again, this indicates that the effect of substitution on the secondary structure might not be predominant, that side chain size could disturb tetramer or later assembly, and that accumulation affects construction of the network, which could have a disturbing influence. However, the dimeric structure does not allow us to see this cumulative process.

Our inducible cell lines allow comparisons between desmin mutants in an isogenic environment. The basic properties of the cell lines (proliferation and inducibility) were similar to cells expressing desWT or desD399Y. In addition, expression levels of the

exogenous proteins are close to or below a ratio of 1:1 with respect to endogenous murine desmin, minimizing the effect of overexpression by maintaining closer-to-physiological conditions. These isogenic contexts enable comparisons of only mutation effects and allow analysis of their behavior in parallel. Random insertion matter could be bypassed with new gene technologies. However, we tested several clones for each mutation to ensure that the observed effect is indeed dependent on mutation and not insertion. Moreover, for R406W mutation, redox effects have been validated in satellite cells from R405W-KI mice. Additionally, these clones present an inducible expression that avoid deleterious effects of overexpression. Finally, it would be interesting to have cells or muscles from patients to confirm these results; unfortunately, they are extremely rare and no samples are currently available for the mutations studied.

Currently to detect desmin point mutations, there is only one specific antibody for R349P. To sense specifically exogenous human desmin, we therefore used a Myc-tag. Indeed, it allows first to quantify (via a shift with desmin antibody) the exogenous desmin vs endogenous and second to detect specifically the human desmin carrying the 6 mutations studied. In addition, we have previously shown that the Myc-tag in N-terminal position, does not cause any alteration in the formation of the WT desmin network *in cellulo*, with or without environment changes (31). Surprisingly, stress did not induce similar aggregation patterns for all 2B mutations as it did in cells expressing the desD399Y mutation. These results suggest that, despite the presence of proline in the rod domain, desA357P-expressing cells are not so sensitive to external stress, unlike desQ389P. These results are similar to those for desS46Y and desS460I, located respectively in the head and tail domains, which were previously shown to have no stress-induced aggregation (33). Our results here show that

desQ389P behaves like desD399Y in terms of aggregate shape and formation upon stress, while desR406W responds to stress to a lesser extent than desQ389P or desD399Y, indicating desR406W may be more sensitive to environmental changes in each experiment. Transient experiments show that all mutations have the same dominant negative effect and lose the ability to form a network without IFs (16,17,37,50). However, our stable clones reveal specific characteristics for each mutation in response to stress. This sensitivity to stress cannot be related to the type of mutation (e.g., proline substitution) or region in the protein (e.g., 2B domain), confirming the variability of aggregate induction mechanisms.

To decipher the underlying molecular mechanisms, we constructed compartment-specific genetically encoded redox reporters. The cyto-Grx1-roGFP2 reporter did not reveal any difference of cytoplasmic GSH/GSSG redox state between C2C12 cells expressing desWT and desD399Y. It is possible that desD399Y expression induces only a slight change of GSH/GSSG ratio that is beyond detection by cyto-Grx1-roGFP2 reporter. Consistently, we were unable to detect any GSSG in C2C12 cells and in our clones by high performance liquid chromatography (data not shown). In contrast, cyto-HyPer reacted differently in cells expressing desWT and in some desmin mutants to oxidative stress-induced aggregation. A significant shift was observed at 60 min, with a greater amount of the oxidized probe found in clones expressing desD399Y and desR406W (Figure 5B). In addition, the delayed return to a normal redox ratio took up to 120 min, especially for the desD399Y clone. Delayed oxidation kinetics related to H_2O_2 metabolism could reflect an imbalanced redox homeostasis in mutant cells, although no H_2O_2 increase was detectable at steady-state. Furthermore, satellite cells extracted from KI-R405W mice exhibited similar results, confirming the implication of redox balance pathways. Finally, observations

745 with mito-HyPer reporter imply that it is the cytoplasmic redox homeostasis that is
746 mostly affected in desmin mutants.

747 Cytoplasmic redox dynamics in response to oxidative stress varied in various
748 mutants. Cells expressing desWT and desQ389P could rapidly restore the redox
749 balance as indicated by HyPer reporter, while cells expressing desD399Y and
750 desR406W required more recovery time. On the other hand, desQ389P and
751 desD399Y displayed similar cellular aggregation. Therefore, these mutants may rely
752 on different altered enzymatic pathways and each mutation may affect specific redox
753 mechanism.

754 Finally, NAC pretreatment induced WT-like results in desD399Y and desR406W
755 cells. As in the case of SEPN1- Knock Out (KO) cells, NAC pretreatment reduces
756 abnormal sensitivity to oxidative stress induced by H_2O_2 (30). Cytoplasmic redox
757 balance related to H_2O_2 content is therefore weakened in the context of D399Y or
758 R406W mutation. We have previously shown that, in cells expressing desD399Y,
759 cadmium chloride (non-oxidative, heavy metal) disturbs the redox dynamic and
760 induces moderate aggregation (33). Therefore, redox homeostasis seems to be
761 fragile in these mutant desmin-expressing cells, so reducing treatment can cause
762 destabilization. This may have deleterious effects on desmin network stability in the
763 context of mutants and NAC would indirectly reduce this sensitivity through
764 glutathione synthesis.

765 Therefore, it may be important for trials of therapeutic molecules to test a wider range
766 of mutations expressed in murine models. Our laboratory has recently experimented
767 with a new type of mouse model that is faster to produce than the KI model. We
768 introduced two desmin mutations (R406W and E413K) into AAV vectors and injected

11-week-old mouse TA muscles (45). Analysis of these muscles showed morphological changes and decreased contractile force, as observed in patients with myofibrillar myopathies. The relatively fast timeline of these experiments suggests an ability to study several mutations in parallel.

The AAVs used in this study were produced by a platform at the National Institute for Health and Medical Research in France, which is different from the laboratory that constructed the desR406W and desE413K viral vectors (45). Differences in transduction may therefore be due to preparation and technical details as well as the individual batch. However, since we injected a maximal volume (70 µL) with respect to muscle size, we could not increase transduction efficiency. So, the variability associated with limited muscle transduction was quite acceptable for a phenotypic study of the impact of desmin over-expression. Indeed as in cells, desmin level remains moderate (Supp. Data 2). Nonetheless, muscle fibers had a very high level of aggregation, up to 90% in fibers expressing exogenous desD399Y, while only a few percent in those expressing desWT. Thus, the location of D399Y is disturbed, similar to patients' muscles, despite expression in an already mature muscle. Moreover, as for the cell lines desD399Y, aggregates are located close to the nuclei like in R406W but not in E413K, shown in a previous study (45). This comparison also applies to SDH staining. In addition, some fibers with aggregates had lighter SDH-stained areas, which could be explained by the low number of mitochondria in this fiber type. In R406W fibers, these non-stained areas are more extensive and seem to affect all fiber types.

As mouse muscles presented pathophysiological characteristics that mimic some of those found in human patients, we treated mice with 20 mM NAC, which is the

commonly used dose for such experiments (49), and higher concentrations seem to have secondary effects on WT mice (unpublished data from our lab). After 1–2 months of NAC pretreatment fibers showed comparable aggregation with or without treatment. Furthermore, NAC increased the number of muscle fibers and decreased their size. Antioxidant supplementation can have a negative impact on acute exercise, suggesting that adaptation to such stress is more dependent on redox homeostasis (51). This is consistent with the role of ROS as intracellular signaling molecules, so the observed hyperplasia may be due to lack of ROS in the presence of NAC, which can have such an effect even without exercise.

Regarding defects in aggregation prevention, one question is whether the dose of NAC was appropriate. We do not have internal markers to ensure NAC was delivered to muscle. However, NAC-treated mice drank less than untreated mice, although no dehydration was observed (Supp. Data 4). This decreased drinking volume could be due to the very low pH of NAC solution or the taste of NAC solution. Nonetheless, the daily NAC dose that mice absorbed remained constant over time. Furthermore, the NAC quantities absorbed in our study were similar to those in other studies, where NAC was effective (e.g., KO-SEPN1 mice) (30). Thus, accessibility of NAC to muscles should have been appropriate in our study.

Another question then arises—why did NAC have no effect in muscle while it prevents D399Y aggregation in cells? Among several hypotheses, one of the most probable is that expression of mutant desmin in the muscle sarcoplasm happens too quickly and/or reaches levels too high for the antioxidant effect to be preventive. Thus, once aggregation has been established, using antioxidant molecules has no effect. NAC treatment may therefore be more appropriate as a first step before

injection, identical to cellular models. However, this experimental course is more difficult to extrapolate to therapy for patients who have the mutation at birth. Alternatively, we could test other anti-aggregative molecules, such as PP242 or NCS 23766, or combine the effects of several molecules, as is done in cell lines (34). An alternative hypothesis is that expression of desD399Y in mature muscles does not initially affect redox balance but may do so in a secondary manner. In that case, studies would need to test the effect of NAC treatment for a longer period of time, for which the KI mouse model could be useful.

Desmin PTMs in both myoblast and muscle contexts were consistent with the absence of network alterations immediately or a few hours after heat shock or oxidative stress. These behaviors indicate that stress is not directly related to aggregation, but that the cellular stress response may be connected to the presence of mutations on soluble-desmin protein or associated in filaments. These results also show singular reactions of desmin to adapt to intrinsic alteration with environmental changes. These changes thus seem to be a post-aggregative process. In fact, aligned spots of the same molecular weight seem to indicate potential known desmin phosphorylations, with some additional for stresses exposition. Nowadays, no other small modifications are described for desmin and it seems here not to participate in early pathophysiological mechanisms. So hyper-phosphorylation 24 h after stress could be one common point. Stress may not depolymerize the desmin network or alter repolymerization in the mutant context (52). Rather, phosphorylation seems to drive the depolymerization/repolymerization process preferentially for aggregated proteins. PTMs with superior weights, seen for desD399Y, could correspond to PTMs known for desmin or other IFs due to short peptides (i.e., ubiquitination or sumoylation). This signal addresses peptides to various degradation processes that

are more complex than proteolysis (ubiquitin proteasome system or autophagy). Alternatively, Olivé et al. (53) found an aberrant form of ubiquitin, UBB+1, that co-localizes with aggregates in skeletal muscles biopsies of patients with myotilinopathy or desminopathy. Other IFs, lamins, and keratins are sumoylated or even hyper-sumoylated under pathological conditions (54). Additional studies could provide a link between these processes in terms of aggregate elimination mechanisms in regards to mutation location.

In the same way, proteolysis related to calpain and caspases could explain the lower-weight forms of desQ389P and desR406W as it has been shown in meat (55). Compared with native desmin isolated from bovine muscle, degradation of oxidized desmin is enhanced by caspases but suppressed by μ-calpain (55). This study also used circular dichroism spectra of desmin to show that oxidation modifies desmin's secondary structure—α-helix content decreased from 76.2% to 52.0%, while random coil content increased from 8.0% to 22.4%.

We did not detect any extra-PTMs in cells or injected muscles, similar to results described for patient muscles (31,32,56). One hypothesis is that no additional PTMs occur, even in desmin aggregates. Indeed, desmin overexpression might overload enzymes and prevent further PTMs. Another hypothesis is that muscle response is delayed and thus may occur at a later timepoint than our observations. However, supplementary PTMs are present in KI-R405W mouse muscles and even untreated satellite cells, suggesting an early effect on desmin PTMs patterns, similar to phosphorylations. Nonetheless, this could be due to an early alteration of redox balance in the homozygous KI context, as has been suggested for linked ROS and PTMs in muscle exercise (57).

Conclusion

Our study demonstrates that redox balance can be altered by expression of at least some desmin mutants. Our results highlight that each mutation has unique pathological molecular mechanisms such as maintaining redox balance and/or protein regulation and aggregation. Therefore, it will be important to integrate these specific behaviors when considering future therapeutics.

ACKNOWLEDGMENTS

We thank Centre d'expérimentation Fonctionnelle (CEF), Pitié Salpétrière Hospital, Paris and the "plateforme d'Hébergement et d'expérimentation animale Buffon" respectivly for AAV-injected and KI-R405W mice. Confocal images were acquired at the imaging facility of the BFA unit. Thanks to Françoise Balter and Philippe Moullier for AAV obtained from Vector Production Center of French National Institute of Health and Medical Research (UMR 1089). We thank Solène Boitard for teaching us the injection method, Dorothée Baïlle and Laurence Vernis for their help in the construction of cyto-HyPer and cyto-Grx1-roGFP2 expression plasmids. We are also grateful to Ana Ferreiro for her constructive advice on muscle physiology and use of NAC. We also thank Elitsa Ivanova for English language improvement. Finally, we acknowledge Linh Chi Bui of the Bioprofiler platform at the BFA unit for her help quantifying GSSG/GSH ratio by HPLC.

FUNDING : F.D., C.H., F.B.R., E.C., A.L., O.A., P.V., and. S.B.P. were supported by Paris Diderot University, the French National Center for Scientific Research (CNRS), and the Agence Nationale de la Recherche (ANR) (3BSV5-0017-DESMECA). This

work was supported by the Association Française contre les Myopathies (AFM) (grant numbers 15454, 18358, and 20802); and ANR (grant number ANR-13-BSV5-0017). S.B.D. is a fellow of AFM.

AUTHOR CONTRIBUTIONS

F.D. and S.B.P. designed the research, performed experiments, analyzed data, and wrote the paper. B.D.S., C.H., F.B.R., E.C., and G.C. performed experiments. M.E.H. provided reporters and analyzed data. P.V. critically read the paper. A.L. extracted muscles from KI-R405 mice, analyzed data, and critically read the paper. O.A. designed AAV experiments.

DECLARATION OF INTEREST

None

Bibliography

1. Strelkov SV, Herrmann H, Aebi U. Molecular architecture of intermediate filaments. BioEssays. 2003 Mar 1;25(3):243–51.
2. Chernyatina AA, Nicolet S, Aebi U, Herrmann H, Strelkov SV. Atomic structure of the vimentin central α-helical domain and its implications for intermediate filament assembly. Proc Natl Acad Sci U S A. 2012 Aug 21;109(34):13620–5.
3. Steinert PM, Idler WW, Cabral F, Gottesman MM, Goldman RD. In vitro assembly of homopolymer and copolymer filaments from intermediate filament subunits of muscle and fibroblastic cells. Proc Natl Acad Sci U S A. 1981 Jun;78(6):3692–6.
4. Reipert S, Steinböck F, Fischer I, Bittner RE, Zeöld A, Wiche G. Association of Mitochondria with Plectin and Desmin Intermediate Filaments in Striated Muscle. Exp Cell Res. 1999 Nov 1;252(2):479–91.
5. Hoffman EP. Desminopathies: Good stuff lost, garbage gained, or the trashman misdirected? Muscle Nerve. 2003;27(6):643–645.
6. Lapouge K, Fontao L, Champliaud M-F, Jaunin F, Frias MA, Favre B, et al. New insights into the molecular basis of desmoplakinand desmin-related cardiomyopathies. J Cell Sci. 2006 Dec 1;119(23):4974–85.
7. Bär H, Strelkov SV, Sjöberg G, Aebi U, Herrmann H. The biology of desmin filaments: how do mutations affect their structure, assembly, and organisation? J Struct Biol. 2004 Nov;148(2):137–52.
8. Clark KA, McElhinny AS, Beckerle MC, Gregorio CC. Striated Muscle Cytoarchitecture: An Intricate Web of Form and Function. Annu Rev Cell Dev Biol. 2002 Nov 1;18(1):637–706.
9. Dalakas MC, Dagvadorj A, Goudeau B, Park K-Y, Takeda K, Simon-Casteras M, et al. Progressive skeletal myopathy, a phenotypic variant of desmin myopathy associated with desmin mutations. Neuromuscul Disord. 2003 Mar;13(3):252–8.
10. Li D, Tapscoft T, Gonzalez O, Burch PE, Quiñones MA, Zoghbi WA, et al. Desmin Mutation Responsible for Idiopathic Dilated Cardiomyopathy. Circulation. 1999 Aug 3;100(5):461.
11. Bär H, Goudeau B, Wälde S, Casteras-Simon M, Mücke N, Shatunov A, et al. Conspicuous involvement of desmin tail mutations in diverse cardiac and skeletal myopathies. Hum Mutat. 2007 Apr 1;28(4):374–86.
12. Batonnet-Pichon S, Behin A, Cabet E, Delort F, Vicart P, Lilienbaum A. Myofibrillar Myopathies: New Perspectives from Animal Models to Potential Therapeutic Approaches. J Neuromuscul Dis. 2017 Feb 28;4(1):1–15.
13. Goldfarb LG, Park K-Y, Cervenakova L, Gorokhova S, Lee H-S, Vasconcelos O, et al. Missense mutations in desmin associated with familial cardiac and skeletal myopathy. Nat Genet. 1998 Aug;19(4):402–3.
14. Muntoni F, Bonne G, Goldfarb LG, Mercuri E, Piercy RJ, Burke M, et al. Disease severity in dominant Emery Dreifuss is increased by mutations in both emerin and desmin proteins. Brain. 2006 May 1;129(5):1260–8.
15. Selcen D, Engel AG. Myofibrillar Myopathy. In: Adam MP, Ardinger HH, Pagon RA, Wallace SE, Bean LJ, Stephens K, et al., editors. GeneReviews® [Internet]. Seattle (WA): University of Washington, Seattle; 2005 [cited 2019 May 13]. Available from: http://www.ncbi.nlm.nih.gov/books/NBK1499/
16. Goudeau B, Rodrigues-Lima F, Fischer D, Casteras-Simon M, Sambuughin N, de Visser M, et al. Variable pathogenic potentials of mutations located in the desmin alpha-helical domain. Hum Mutat. 2006 Sep 1;27(9):906–13.

17. Bär H, Mücke N, Kostareva A, Sjöberg G, Aebi U, Herrmann H. Severe muscle disease-causing desmin mutations interfere with in vitro filament assembly at distinct stages. Proc Natl Acad Sci U S A. 2005 Oct 18;102(42):15099–104.
18. Clemen ChristophS, Herrmann H, Strelkov SergeiV, Schröder R. Desminopathies: pathology and mechanisms. Acta Neuropathol (Berl). 2013 Jan 1;125(1):47–75.
19. Rappaport L. Storage of phosphorylated desmin in a familial myopathy. FEBS Lett. 1988;231:421–5.
20. Schröder R, Goudeau B, Simon MC, Fischer D, Eggermann T, Clemen CS, et al. On noxious desmin: functional effects of a novel heterozygous desmin insertion mutation on the extrasarcomeric desmin cytoskeleton and mitochondria. Hum Mol Genet. 2003 Mar 15;12(6):657–69.
21. Bouvet M, Dubois-Deruy E, Alayi TD, Mulder P, El Amranii M, Beseme O, et al. Increased level of phosphorylated desmin and its degradation products in heart failure. Biochem Biophys Rep. 2016 Jul;6:54–62.
22. Milner DJ, Weitzer G, Tran D, Bradley A, Capetanaki Y. Disruption of muscle architecture and myocardial degeneration in mice lacking desmin. J Cell Biol. 1996 Sep 1;134(5):1255–70.
23. Li Z, Colucci-Guyon E, Pinçon-Raymond M, Mericskay M, Pournin S, Paulin D, et al. Cardiovascular Lesions and Skeletal Myopathy in Mice Lacking Desmin. Dev Biol. 1996 May 1;175(2):362–6.
24. Kostareva A, Sjöberg G, Bruton J, Zhang S-J, Balogh J, Gudkova A, et al. Mice expressing L345P mutant desmin exhibit morphological and functional changes of skeletal and cardiac mitochondria. J Muscle Res Cell Motil. 2008 Jan 1;29(1):25–36.
25. Winter L, Wittig I, Peeva V, Eggers B, Heidler J, Chevessier F, et al. Mutant desmin substantially perturbs mitochondrial morphology, function and maintenance in skeletal muscle tissue. Acta Neuropathol (Berl). 2016;132:453–73.
26. Radak Z, Chung HY, Goto S. Systemic adaptation to oxidative challenge induced by regular exercise. Free Radic Exerc. 2008 Jan 15;44(2):153–9.
27. Lew H, Pyke S, Quintanilha A. Changes in the glutathione status of plasma, liver and muscle following exhaustive exercise in rats. FEBS Lett. 1985 Jun 17;185(2):262–6.
28. Mason SA, Morrison D, McConell GK, Wadley GD. Muscle redox signalling pathways in exercise. Role of antioxidants. Hum Perform Redox Signal Health Dis. 2016 Sep 1;98:29–45.
29. Moulin M, Ferreiro A. Muscle redox disturbances and oxidative stress as pathomechanisms and therapeutic targets in early-onset myopathies. Semin Cell Dev Biol. 2017;64:213–23.
30. Arbogast S, Dill C, Ramahefasolo C, Piemonte F, Serreri C, Lescure A, et al. N-acetylcysteine as an effective treatment in vivo and identification of biomarkers in SEPN1-related myopathy: A first preclinical trial. Neuromuscul Disord. 2014;24(9):1032–7.
31. Janué A, Olivé M, Ferrer I. Oxidative Stress in Desminopathies and Myotilinopathies: A Link between Oxidative Damage and Abnormal Protein Aggregation. Brain Pathol. 2007 Oct 1;17(4):377–88.
32. Janué A, Odena MA, Oliveira E, Olivé M, Ferrer I. Desmin Is Oxidized and Nitrated in Affected Muscles in Myotilinopathies and Desminopathies. J Neuropathol Exp Neurol [Internet]. 2007;66(8). Available from: http://journals.lww.com/jneuropath/Fulltext/2007/08000/Desmin_Is_Oxidized_and_Nitrated_in_Affected.5.aspx
33. Segard B-D, Delort F, Bailleux V, Simon S, Leccia E, Gausseres B, et al. N-Acetyl-L-Cysteine Prevents Stress-Induced Desmin Aggregation in Cellular Models of Desminopathy. PLoS ONE. 2013 Oct 1;8(10):e76361.

34. Cabet E, Batonnet-Pichon S, Delort F, Gausserès B, Vicart P, Lilienbaum A. Antioxidant Treatment and Induction of Autophagy Cooperate to Reduce Desmin Aggregation in a Cellular Model of Desminopathy. Wiche G, editor. PLoS ONE. 2015;10(9):e0137009.
35. Hnia K, Ramspacher C, Vermot J, Laporte J. Desmin in muscle and associated diseases: beyond the structural function. Cell Tissue Res. 2014 Oct 31;1–18.
36. Weber K, Geisler N. Intermediate Filaments: Structural Conservation and Divergence. Ann N Y Acad Sci. 1985;455(1):126–143.
37. Dagvadorj A, Olivé M, Urtizberea J-A, Halle M, Shatunov A, Bönnemann C, et al. A series of West European patients with severe cardiac and skeletal myopathy associated with a de novo R406W mutation in desmin. J Neurol. 2004 Feb 1;251(2):143–9.
38. Pruszczyk P, Kostera-Pruszczyk A, Shatunov A, Goudeau B, Dramiñska A, Takeda K, et al. Restrictive cardiomyopathy with atrioventricular conduction block resulting from a desmin mutation. Int J Cardiol. 2007 Apr 25;117(2):244–53.
39. Herrmann H, Aebi U. Intermediate filaments and their associates: multi-talented structural elements specifying cytoarchitecture and cytodynamics. Curr Opin Cell Biol. 2000 Feb 1;12(1):79–90.
40. Strelkov SV, Burkhard P. Analysis of α-Helical Coiled Coils with the Program TWISTER Reveals a Structural Mechanism for Stutter Compensation. J Struct Biol. 2002 Jan 1;137(1):54–64.
41. Snider NT, Omary MB. Post-translational modifications of intermediate filament proteins: mechanisms and functions. Nat Rev Mol Cell Biol. 2014 Mar;15(3):163–77.
42. Ohanna M, Sobering AK, Lapointe T, Lorenzo L, Praud C, Petroulakis E, et al. Atrophy of S6K1(-/-) skeletal muscle cells reveals distinct mTOR effectors for cell cycle and size control. Nat Cell Biol. 2005 Mar;7(3):286–94.
43. Belousov VV, Fradkov AF, Lukyanov KA, Staroverov DB, Shakhbazov KS, Terskikh AV, et al. Genetically encoded fluorescent indicator for intracellular hydrogen peroxide. Nat Meth. 2006 Apr;3(4):281–6.
44. Gutscher M, Pauleau A-L, Marty L, Brach T, Wabnitz GH, Samstag Y, et al. Real-time imaging of the intracellular glutathione redox potential. Nat Methods. 2008 Jun;5(6):553–9.
45. Joanne P, Chourbagi O, Hourde C, Ferry A, Butler-Browne G, Vicart P, et al. Viral-mediated expression of desmin mutants to create mouse models of myofibrillar myopathy. Skelet Muscle. 2013;3(1):4.
46. Strelkov SV, Herrmann H, Geisler N, Wedig T, Zimbelmann R, Aebi U, et al. Conserved segments 1A and 2B of the intermediate filament dimer: their atomic structures and role in filament assembly. EMBO J. 2002 Mar 15;21(6):1255–66.
47. Salo DC, Donovan CM, Davies KJA. HSP70 and other possible heat shock or oxidative stress proteins are induced in skeletal muscle, heart, and liver during exercise. Free Radic Biol Med. 1991 Jan 1;11(3):239–46.
48. MacArthur MW, Thornton JM. Influence of proline residues on protein conformation. J Mol Biol. 1991 Mar 20;218(2):397–412.
49. Chourbagi O, Bruston F, Carinci M, Xue Z, Vicart P, Paulin D, et al. Desmin mutations in the terminal consensus motif prevent synemin-desmin heteropolymer filament assembly. Exp Cell Res. 2011 Apr 1;317(6):886–97.
50. Goudeau B, Dagvadorj A, Rodrigues-Lima F, Nédellec P, Casteras-Simon M, Perret E, et al. Structural and functional analysis of a new desmin variant causing desmin-related myopathy. Hum Mutat. 2001 Nov 1;18(5):388–96.
51. Merry TL, Ristow M. Do antioxidant supplements interfere with skeletal muscle adaptation to exercise training? J Physiol. 2016 15;594(18):5135–47.

52. Winter L, Staszewska I, Mihailovska E, Fischer I, Goldmann WH, Schröder R, et al. Chemical chaperone ameliorates pathological protein aggregation in plectin-deficient muscle. J Clin Invest. 2014 Mar 3;124(3):1144–57.
53. Olivé M, Armstrong J, Miralles F, Pou A, Fardeau M, Gonzalez L, et al. Phenotypic patterns of desminopathy associated with three novel mutations in the desmin gene. Neuromuscul Disord NMD. 2007 Jun;17(6):443–50.
54. Snider NT, Weerasinghe SVW, Iñiguez-Lluhí JA, Herrmann H, Omary MB. Keratin Hypersumoylation Alters Filament Dynamics and Is a Marker for Human Liver Disease and Keratin Mutation. J Biol Chem. 2011 Jan 21;286(3):2273–84.
55. Chen Q, Huang J, Huang F, Huang M, Zhou G. Influence of oxidation on the susceptibility of purified desmin to degradation by μ-calpain, caspase-3 and -6. Food Chem. 2014 May 1;150:220–6.
56. Marini M, Guglielmi V, Faulkner G, Piffer S, Tomelleri G, Vattemi G. Immunoblot as a potential diagnostic tool for myofibrillar myopathies. ELECTROPHORESIS. 2015;36(24):3097–3100.
57. Powers SK, Radak Z, Ji LL. Exercise-induced oxidative stress: past, present and future. J Physiol. 2016 15;594(18):5081–92.

Supporting Information

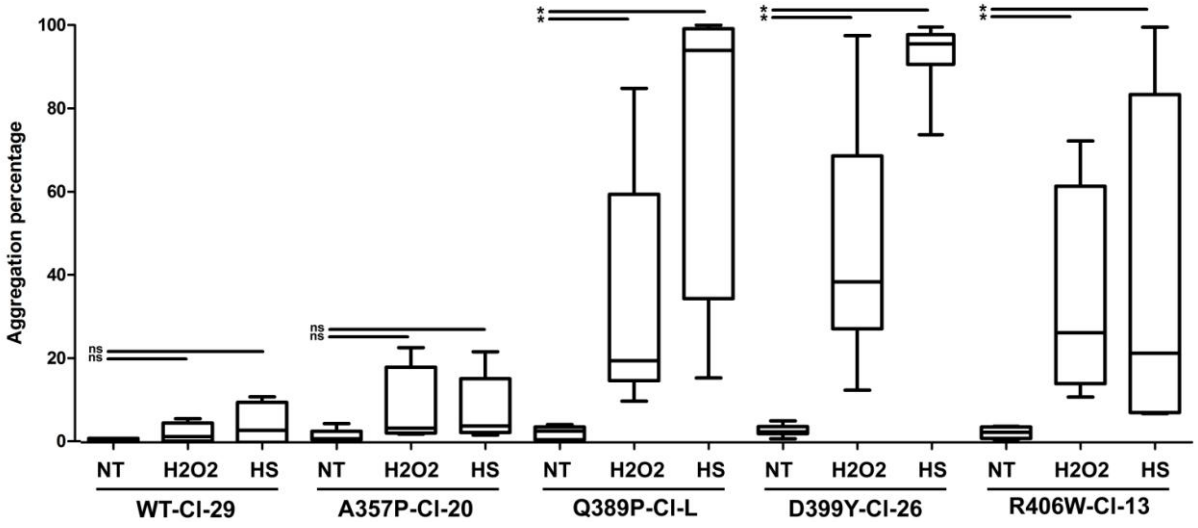

Supp. Data 1: Box plot representing the aggregation percentages 24 h after stress (T24) compared to untreated cells. Three different treatments are shown: heat shock (HS), oxidative stress (H_2O_2), and no stress (NT). Cells were counted in at least 3 independent experiments (>100 cells each) (ns: not significant; *$p < 0.05$, compared to unstressed).

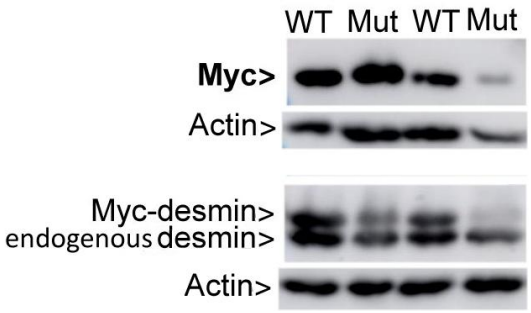

Supp. Data 2: Desmin expression levels in AAV-infected muscles. Representative Western blot analysis of endogenous and human Myc-desmin in muscles injected with AAV expressing WT or D399Y (Mut) desmin. Actin serves as a loading control.

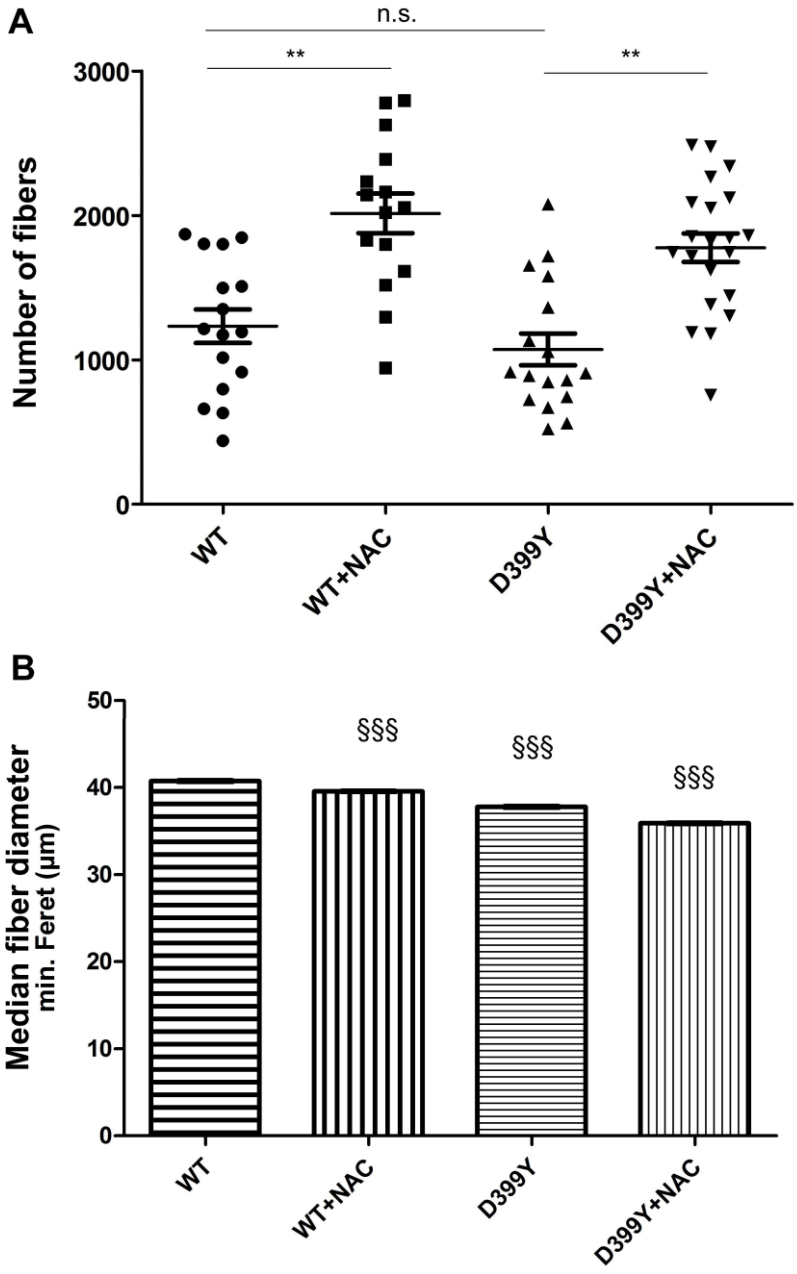

Supp. Data 3: Effect of NAC on fiber number and median fiber diameter in TA muscles expressing ectopic human desmin. (A) Quantification of number of fibers in TA muscles expressing WT or D399Y mutant desmin, untreated or treated with NAC. Plot shows the average of the total number of fibers in 4 sections from 4 injected muscles for each condition (n.s.: $p > 0.05$; **: $p < 0.01$). (B) Quantification of median fiber diameters (min. Feret values) in TA muscles expressing WT or D399Y mutant desmin, untreated or treated with NAC. Diameters were measured on whole muscle transversal sections stained with laminin. Medians were calculated with 5 sections from 3 injected muscles for each condition (§§§: $p < 0.001$, each construct compared to others).

Treatment	Mean volume drank (mL/day)	Ratio volume drank (without NAC/with NAC)	Mean absorbed NAC (mg/mouse/day)	Mean absorbed NAC (g/kg/day)
Without NAC 1 month	4.53	1.3	–	–
With NAC 1 month	3.45	–	11.5	0.38
Without NAC 2 months	5.68	1.9	–	–
With NAC 2 months	2.97	–	10	0.33

Supp. Data 4: Measures of amount drank by mice. Amount of liquid (water or NAC solution) drank by mice after 1 or 2 months. Each group contains an equivalent number of animals injected with AAV expressing WT or D399Y mutant desmin.